universität wien

MASTERARBEIT / MASTER'S THESIS

Titel der Masterarbeit / Title of the Master's Thesis

„Analysis of Interleukin-1β, Interleukin-1β Receptor and Caspase-1 in Rasmussen's Encephalitis"

verfasst von / submitted by

Lic. Lucía Quemada Garrido

angestrebter akademischer Grad / in partial fulfilment of the requirements for the degree of

Master of Science (MSc)

Vienna, 2017

Studienkennzahl lt. Studienblatt / degree programme code as it appears on the student record sheet:	A 066 830
Studienrichtung lt. Studienblatt / degree programme as it appears on the student record sheet:	Masterstudium Molekulare Mikrobiologie, Mikrobielle Ökologie und Immunbiologie
Betreut von / Supervisor:	Ao.Univ.Prof. Dr. Jan Bauer

Table of Contents

Acknowledgments

First of all I would like to thank my supervisor Prof. Dr. Jan Bauer for giving me the opportunity to do my master thesis in his lab group. I am very thankful for all the knowledge and excellent ideas he shared with me, as well as for his guidance through this thesis. It was a pleasure to work with him.

My special gratitude belongs to Anna Tröscher, MSc, for guiding me during my thesis. Thank you for teaching me a lot of new things that I used in my project and for being patient when it was needed but also encouraging in many other moments. She is a great colleague but even more a great person.

Further, I want to thank Prof. Dr. med. Christian G. Bien from the Epilepsy Center in Bethel for providing the working samples.

I want to acknowledge Ulrike Köck, Marianne Leisser and Angela Kury for their technical assistance and for sharing with me their extensive knowledge in histochemistry during my experiments. My thanks also go to Markus Jeitler of the Core Facilities of the Medical University of Vienna for performing the RNA quality and quantity determination.

Furthermore, I want to thank all my colleagues and other professors from the department of Neuroimmunology for being always ready to help and giving good advises. Especially, I want to mention Joana Santos, Isabella Wimmer and Bleranda Zeka for sharing their scientific knowledge with me but also their personal experiences in our free time. The time I shared with you will be always positive memory.

Most of all I want to express my deep gratitude to my family and friends for always encouraging me and believing in me. Thank you mum for being always next to me in every decision I make, supporting me and loving me. Thank you Tamás for reminding me every day that we have to fight for our dreams and celebrate every small achievement.

1 Abstract

Rasmussen Encephalitis (RE) is a rare progressive epileptic disorder with unknown etiology (Thompson and Tsirka, 2017). It is characterized by unilateral hemispheric inflammation, drug-resistant focal epilepsy and progressive neurological and cognitive deterioration (Varadkar et al., 2014).

Inflammatory mediators, such as cytokines like interleukin 1β (IL-1β), have been shown to be highly epileptogenic in animal models (Teresa Ravizza et al., 2006). However, little is known about the role of IL-1β in the course of RE. To analyze the presence and cell-type localization of IL-1β and its receptor interleukin 1 receptor 1 (IL-1R1) formalin-fixed paraffin-embedded (FFPE) and cryo tissues were used from human RE patients and controls. Firstly, the amount of IL-1β was analyzed by western blot but the results revealed only the detection of the control protein β-actin but not the cytokine. Therefore, we decided to determine the amount of IL-1β and IL-1R1 by real-time quantitative polymerase chain reaction (qPCR) as well as by immunohistochemical (IHC) stainings and cell countings for IL-1β. Moreover we analyzed the cell-type specific expression of IL-1β, IL-1R1 and Caspase-1, an enzyme which plays a key role in the production of IL-1β by double and triple confocal fluorescence stainings with markers for astrocytes (GFAP), microglia (Iba-1 and CD68) and neurons (NeuN).

The qPCR data revealed that at all stages RE patients have a significantly higher expression of IL-1β and IL-1R1 mRNA compared to controls. Furthermore we could confirm the results obtained by qPCR by showing the presence of IL-1β in RE by immunhistochemistry and quantification of IL-1β positive cells. Our confocal fluorescence stainings showed that IL-1β and Caspase-1 were expressed in microglia but not in astrocytes, with Caspase-1 positive cells being more abundant than IL-1β positive cells. IL-1R1 on the other hand was expressed in microglia as well as in astrocytes and neurons. This study shows the upregulation of the cytokine in RE and reveals a possible role of IL-1β in this disease. Moreover, it provides a better understanding of the cells in the Central Nervous System (CNS) that express IL-1β, IL-1R1 and Caspase-1 and therefore contributes to a better understanding of the function of these cells in human pathology.

2 Zusamenfassung

Rasmussen Enzephalitis (RE) ist eine seltene progressive Form der Epilepsie mit unbekannter Ätiologie. Die Hauptcharakteristika sind unilaterale hemisphärische Entzündung, arzneimittelresistente fokale Epilepsie und progressive neurologischer und kognitiver Verfall.

In Tiermodellen wurde gezeigt, dass entzündliche Faktoren, wie beispielsweise Interleukin 1β (IL-1β), hoch epileptogen sind. Nichts desto trotz, ist noch wenig über die Rolle von IL-1β in RE bekannt. Um diese Frage zu beantworten, wurde die Menge an IL-1β sowie dessen Rezeptor, Interleukin 1 Rezeptor 1 (IL1-R1) in verschiedenen Stadien der RE sowie in Kontrollgewebe bestimmt. Außerdem wurde anhand von Formalin fixierten, Paraffin eingebetteten (FFPE) sowie Cryo Gewebe histologische Auswertung der genauen Zelltypen, die oben genannten Proteine exprimieren, festgestellt. Zuerst wurde eine Proteinmengenbestimmung mittels Western Blot durchgeführt, um die genaue Menge von IL-1β zu evaluieren. Die IL-1β Menge befand sich unter dem Detektionslimit, da nur die Kontrollproteine aber nicht IL-1β detektiert werden konnten. Daraufhin wurde das Expressionslevel des Zytokines IL-1β sowie dessen Rezeptor mittels qPCR bestimmt. Zusätzlich wurden immumohistochemische Färbungen für IL-1β quantitative ausgewertet. Zusätzlich wurden mittels Doppel- beziehungsweise Trippelmarkierungen Zelltyp spezifische Lokalisation von IL-1β, IL1R1 sowie Caspase-1, ein Enzyme involviert in IL-1β Aktivierung und Sekretion, mittels Konfokalem Laser Mikroskop bestimmt. Dafür wurden Marker für Astrozyten (GFAP), Mikroglia (Iba-1 und CD68) und Neuronen (NeuN) verwendet.

Die Expressionslevel Analysen zeigten, dass IL-1β sowie IL1-R1 in allen Stadien der RE im Vergleich zu den Kontrollen deutlich aufreguliert sind. Diese Daten wurden mittels immunohistochemischer Quantifizierung für IL-1β validiert. Die Konfokal Laser Mikroskop Analysen zeigten auf, dass IL-1β sowie Caspase-1 in Mikroglia sowie Astrozyten expremiert wird und Caspase-1 um einiges häufiger vorhanden ist als IL-1β. IL1-R1 wird auf Mikroglia sowie Astrozyten und auch Neuronen exprimiert.

Diese Studie zeigt die drastische Aufregulierung von IL-1β sowie IL1-R1 in RE und weist auf eine mögliche Rolle des Zytokines in dieser Krankheit hin. Außerdem zeigt diese Arbeit auf, welche Zelltypen die jeweiligen Proteine exprimieren und gibt dadurch einen besseren Einblick in die Funktion dieser Zellen in humaner Pathologie.

3 Introduction

The innate immune system (IS*)* develops at an early stage of life and provides the first line of defense in a generic way against invading pathogens and eventually it is sufficient to clear the infection (Matin et al., 2015). Tissue-resident macrophages, dendritic cells, mast cells, circulating phagocytes and complement molecules are the main components of the innate immune response (Waisman et al., 2015). However, the adaptive IS is triggered when the innate IS is not sufficient as the later phase of host defense and it responds specifically to antigens on different pathogens in addition to incorporating immunological memory through a mechanism of gene rearrangement (Matin et al., 2015). In this case, specific B- and T-cells are activated for pathogen clearance (Waisman et al., 2015).

Remarkable investigations have been done in the last decade to understand how the innate IS identifies pathogens, and how this leads to the activation of signaling pathways that result in the transcriptional regulation of immune response genes including pro-inflammatory cytokines such IL-1β, type 1 interferon, tumor necrosis factor-α (TNF-α), antimicrobial peptides, and adhesion molecules (Bryant and Fitzgerald, 2009; Chen et al., 2009).

The major way by which the innate immune system deals with infections and tissue injury is to stimulate acute inflammation, which is frequently triggered by pathogen-associated molecular patterns (PAMPs) (Orozco LD, Bennett BJ, Farber CRChe et al., 2012) and damage-associated molecular patterns (DAMPs) on infectious agents or disease-associated host molecules by pattern-recognition receptors (PRRs) (Becker, 2006; Jha et al., 2015) localized on tissue- resident macrophages, dendritic cells, mast cells, circulating phagocytes and a variety of sentinel cells (Antonelli and Kushner, 2017; Waisman et al., 2015). It is comprised mainly of polymorphonuclear cells, natural killer (NK) cells and monocytes (Becker, 2006). The ultimate goal of inflammation is to reinstate the optimal metabolic homeostatic state (Antonelli and Kushner, 2017). In contrast, chronic inflammation takes place when acute inflammation persists due to non-degradable pathogens, viral infection, importunate foreign bodies, or autoimmune reactions. The prolonged pathological condition leads to a progressive shift in the type of cells present at the site of inflammation, such as mononuclear immune cell infiltration (monocytes, lymphocytes, macrophages and plasma cells) and it is characterized also by tissue destruction and fibrosis (Khansari et al., 2009).

3.1 Inflammation in the Central Nervous System (CNS)

The brain has traditionally been considered an immune-privileged site because of the blood-brain barrier (BBB), the lack of a conventional lymphatic system, and the limited trafficking of peripheral immune cells. However, there is now a lot of evidence that innate as much as adaptive immune responses can occur within the CNS in response to pathogens invasion, self-

antigens or tissue damage of several etiologies. Astrocytes, microglia, BBB endothelial cells and peripheral immune cells extravasating into the brain parenchyma can all produce pro-inflammatory and anti-inflammatory cytokines (Vezzani et al., 2011).

Under physiological conditions the BBB limits the movement of cells and macromolecules between the blood and CNS tissue, and the CNS is under tight surveillance by the immune system against pathogens or aberrant cells (Waisman et al., 2015). During systemic inflammation the BBB becomes more permeable, antibodies as well as peripheral immune cells and inflammatory molecules that can contribute to brain pathology may penetrate the BBB through different mechanisms (Figure 1). This process is called neuroinflammation (Zhou et al., 2016) and the brain resident microglia as part of the neuroinflammation are able to trigger an appropriate response involving production and release of inflammatory cytokines (e.g. IL-1β), chemokines, and other immunologically active peptides, resulting in the activation of astrocytes and further recruitment of peripheral immune cells (Gustin et al., 2015; Sankowski et al., 2015). Among the inflammatory responses, IL-1β secretion has been shown to have important functions in diseases of the CNS, yet its production and mechanism of action is not fully understood and its precise implication in neuroinflammatory diseases needs further investigation (Gustin et al., 2015).

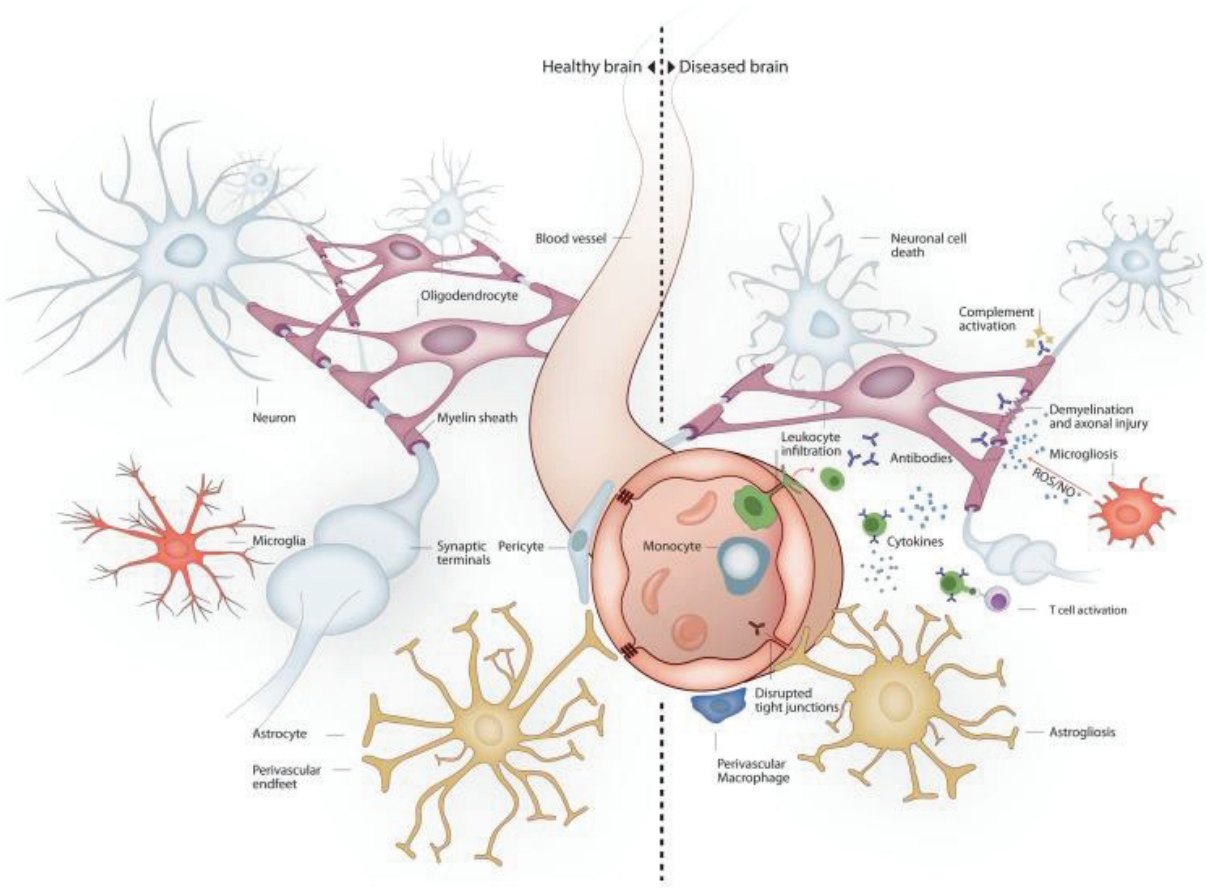

Figure 1. Brain environment changes in response to systemic inflammation. *Under healthy conditions the main cell types in the brain are neurons, oligodendrocytes, astrocytes and microglia.*

Neurons connect to each other through long axonal processes with synapses. Oligodendrocytes support axons with myelin sheaths. Astrocytes interact with blood vessels to form the blood-brain barrier and maintain neuronal synapses. Microglia form long processes that surveillance the brain and phagocyte apoptotic cells and cut inactive synapses without initiation of inflammation. Under inflammatory conditions some mechanisms lead to neurodegeneration. Peripheral immune cells and inflammatory molecules cross over the blood-brain barrier exerting direct and indirect neuronal toxicity. Oligodendroglial myelin sheaths can be affected leading to axonal degeneration. Astrocytosis leads to reduced blood-brain barrier and synaptic maintenance. Microgliosis leads to a pro-inflammatory microglial phenotype with reduced phagocytic and tissue maintenance functions (Sankowski et al., 2015).

Non-specific CNS inflammation is postulated to contribute to pathology in a host of neurologic diseases, some acute and some chronic (Becker, 2006). The antibodies are directed towards an antigen or against a pathogen that mimics a CNS antigen. It is also probable that pathogenic autoantibodies were formed directly against CNS antigens that were successfully presented to the immune system during the progression of a CNS insult (Becker, 2006). Markers of CNS autoimmunity are found in many neurological diseases, such as Alzheimer's disease, vascular dementia, Parkinson's disease, Rasmussen's encephalitis, epilepsia partialis continue and multiple sclerosis (Becker, 2006; Berger et al., 2003; Bien et al., 2002; Rogers et al., 1994; Takahashi et al., 2003).

3.1.1 Inflammation and epilepsy

Epilepsy is one of the most common chronic brain disorders worldwide and is characterized by recurrent unprovoked epileptic seizures with cognitive, neurobiological and psychosocial consequences due to abnormal, hyperexcitability and synchronized firing of groups of neurons, blood brain barrier breakdown and neuronal loss (Matin et al., 2015; Vezzani et al., 2011). Both innate and adaptive immunity have been implicated in epilepsy, and microglia, astrocytes and neurons are considered to contribute to the innate immunity-type processes that cause inflammation of the brain. Nevertheless, the etiology of epilepsy is not completely understood and pharmacological therapies fail in about 30% of the epilepsy cases (Vezzani et al., 2011).

While the ultimate effectors of seizures are neurons, recent experimental studies and pathological analyses of patient brain tissue revealed that neuroinflammation and inflammatory processes play an important role in the pathophysiology of epilepsy and convulsive disorders (Marchi et al., 2014; Matin et al., 2015). Several established and novel mechanisms could mediate the effects of inflammatory mediators on neuronal excitability and epilepsy (Figure 2) (Vezzani et al., 2011). Some of these processes could be involved in the precipitation and recurrence of seizures, while others are implicated in the development of

epileptogenesis. Experimental studies in rodent models have revealed that seizures activity intrinsically can trigger brain inflammation. In addition, seizures may perpetuate chronic inflammation. However, cell loss associated to seizures can contribute to inflammation but is not a requirement for inflammation to happen. Additionally, models of CNS infections suggested that pre-existing brain inflammation increases the predisposition to seizures, associated with excitability of neurons (Vezzani et al., 2011).

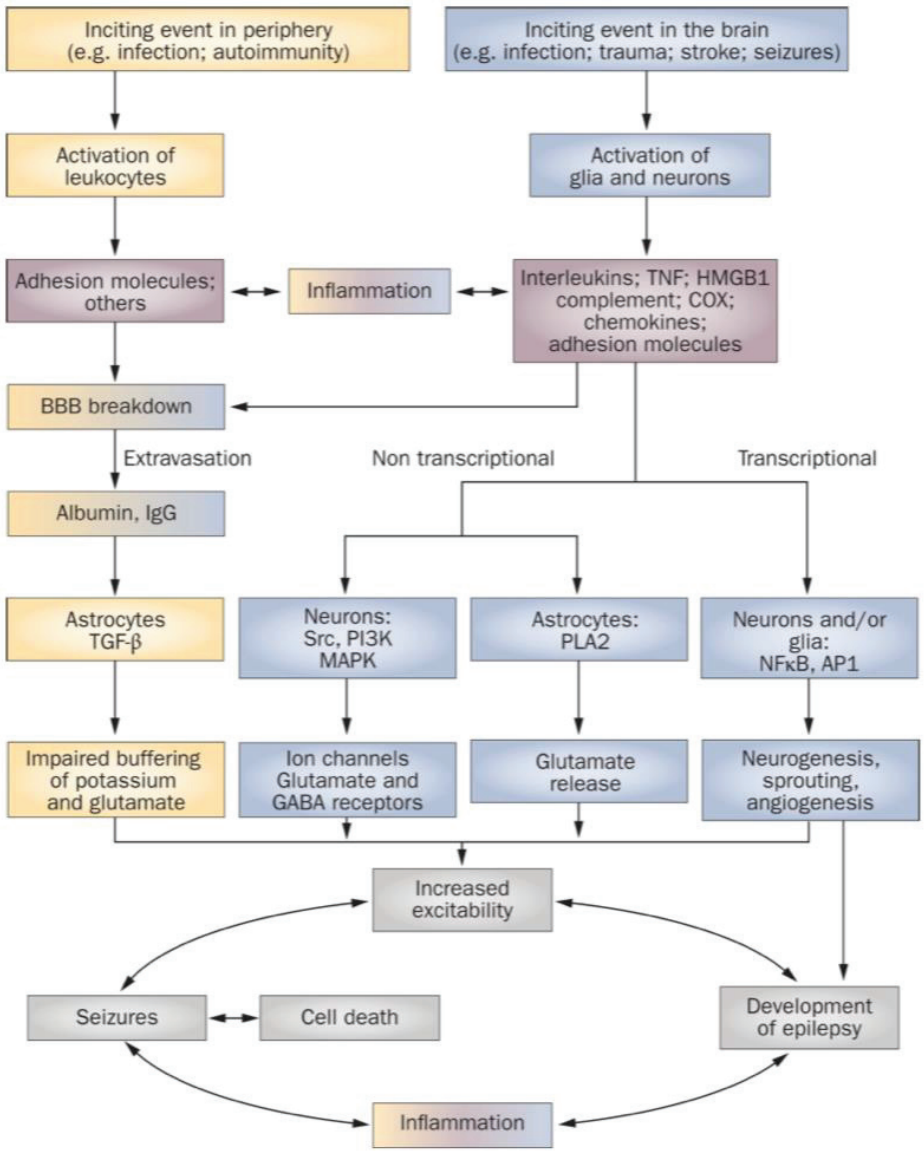

Figure 2. Pathophysiological cascade of inflammatory events in epilepsy. *Pathological events initiated in the CNS by local injuries, or peripherally following infections or as a result of autoimmune disorder, can lead to activation of brain cells or leukocytes, respectively. These cells release inflammatory molecules into the brain or blood, thereby eliciting a cascade of inflammatory events that cause a spectrum of physiopathological outcomes. The effects of brain inflammation contribute to the generation of individual seizures and cell death, which, in turn, activates further inflammation, thereby establishing a vicious circle of events that contributes to the development of epilepsy. In yellow the peripheral pathway, in blue the CNS pathway, and in pink the inflammatory molecules. The*

merged colors indicate the contribution of each pathway to inflammation and BBB damage. AP1, activator protein 1; BBB, blood– brain barrier; COX, cyclooxygenase; GABA, γ-aminobutyric acid; HMGB1, high-mobility group box 1; MAPK, mitogen-activated protein kinase; NFκB, nuclear factor kappa B; PI3K, phosphatidylinositol-4,5-bisphosphate 3-kinase; PLA2, phospholipases A2; TGF-β, transforming growth factor β; TNF, tumor necrosis factor (Vezzani et al., 2011).

In the last decade, experimental evidence in animal models has supported the idea of the reciprocal causal links between inflammation and epilepsy. Recurrent short seizures or single prolonged seizures were induced in adult rats and mice and resulted in a rapid induction of inflammatory mediators in brain regions of seizure activity onset and propagation. Immunohistochemical studies on rodent brains also demonstrated the presence of waves of inflammation triggered by the induction of the status epilepticus during the epileptogenic process (Vezzani et al., 2011). Brain tissue from rodents with experimental chronic temporal lobe epilepsy contains activated microglia and astrocytes expressing inflammatory molecules (Ravizza et al., 2008). Other evidence supports the idea that inflammation causes seizures. Clinical evidence indicates that steroids and other anti-inflammatory treatments display anticonvulsant activity in some drug-resistant human epilepsies. Additional data shows that febrile seizures are often caused by an increase in the levels of pro-inflammatory molecules. Moreover, inflammatory mediators have been detected in surgically excised brain tissue from patients suffering from temporal lobe epilepsy and cortical dysplasia-related epilepsy. Finally, systemic injection of lipopolysaccharide in the periphery and in the brain of a rat model has been shown to lower seizure threshold in the short and long term (Vezzani et al., 2011).

The cycle of seizures inducing inflammation and inflammation exacerbating seizures highlights the potential benefit of targeting components of the inflammatory cascade to stop this cycle and to treat seizures and epilepsy (Edye et al., 2014).

Among the epileptogenic mechanisms investigated in animal models, glial cells are considered as key contributors in seizure-prone areas to neuronal circuit hyperexcitability resulting in seizures (Vezzani, 2015). Epileptogenesis activates microglia and astrocytes which increase their synthesis and release of soluble neurotrophic or neurotoxic molecules, including pro-inflammatory molecules and anti-inflammatory cytokines and contributes to the generation of neuroinflammation (Matin et al., 2015; Scott et al., 2016; Vezzani, 2015; Vezzani et al., 2011). The scope of microglia and astrocytes activation correlates with the duration of epilepsy and the frequency of spontaneous seizures in animal models, as well as in humans (Devinsky et al., 2017; T. Ravizza et al., 2006). Moreover cell-specific expression of inflammatory molecule's cognate receptors has been observed in neurons, glia, as well as in brain microvessels. It is suggested that these soluble inflammatory mediators mediates autocrine and paracrine functional loops among different brain-resident cell populations (Vezzani, 2015). As a consequence of neuroinflammation, immune cells from the periphery (e.g. lymphocytes) may be recruited into the brain parenchyma (Marchi et al., 2014).

3.2 The Inflammasomes

As mentioned above, in this project we focused on the role of the pro-inflammatory cytokine IL-1β in RE, a type of cortical encephalitis associated with epilepsy (Bauer and Bien, 2009). Preclinical data suggest that direct targeting of IL-1β, might be warranted, because this mechanism could contribute to different type of seizures (Vezzani et al., 2011).

In view to understand the role played by IL-1β in neuroinflammatory chronic diseases, it is essential to characterize in detail the inflammasome expression and activation in CNS inflammatory cells.

Inflammasomes are high molecular weight cytosolic multiprotein complexes associated with the innate immune inflammatory responses by triggering the activation of inflammatory caspases and subsequently the maturation of proinflammatory cytokines IL-1β and IL-18 as a result of recognition of foreign or endogenous danger signals (Schroder and Tschopp, 2010; Waisman et al., 2015; Zhou et al., 2016). Another function of the inflammasome is the regulation of pyroptosis, a Caspase-1-dependent form of cell death that is highly inflammatory (Bryant and Fitzgerald, 2009; Guo et al., 2015). The inflammasomes are identified as part of the foundation of the intracellular surveillance system. The factors that initiate inflammasome assembly decide the exact composition of an inflammasome (Jha et al., 2015) (Figure 3).

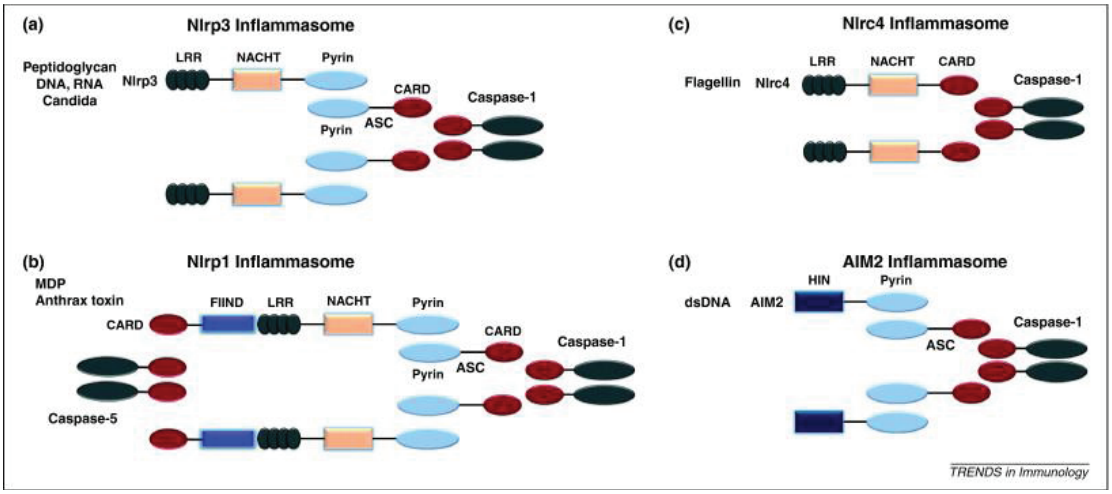

Figure 3. Schematic representation of the four best-described inflammasomes*. (a) The NLRP3 inflammasome activates Caspase-1 by recruiting ASC. (b) The NLRP1 inflammasome has a FIIND and CARD domain in addition to its LRR, NACHT and Pyrin domains and can recruit Caspase-5. (c) The NLRC4 inflammasome has a CARD domain that can directly recruit pro-Caspase-1. (d) The AIM2 inflammasome consists of a Pyrin and DNA-binding HIN domain that forms a complex with ASC and Caspase-1. ASC: apoptosis-associated speck-like protein containing a CARD; FIIND: function to find domain; LRR: leucine-rich repeat; AIM2: absent in melanoma 2; MDP: muramyl dipeptide* (van de Veerdonk et al., 2011).

Inflammasomes contain PRRs that respond to danger signals through the detection of PAMPs linked to microbes and DAMPs produced during tissue-based injury (Freeman and Ting, 2016; Zhou et al., 2016). The PRR contains a central nucleotide-binding and oligomerisation (NACHT) domain, a C-terminus leucine rich repeat (LRR) for ligand sensing and autoregulation, and a N-terminus Caspase activation and recruitment domain (CARD) or pyrin domain (PYD) for binding adaptor and effector proteins. The type and combination of these components defines the inflammasome formed (Edye et al., 2014).

Until now, two different types of inflammasomes have been described. The first type is the inflammasomes that use the NOD-like receptors such as NLRP1, NLRP2, NLRC4. The best-characterized inflammasome is the NLRP3 inflammasome. The other type of inflammasomes uses AIM2 which is a non-NLR inflammasome receptor and it is a member of the PYHIN family (**Figure 3**) (Freeman and Ting, 2016; Martinon et al., 2002). Although all of them are activated through different mechanisms and stimuli, their activation always triggers Caspase-1 and consequently IL-1β and IL-18.

In the brain several cell types express specialized PRRs such as Toll-like receptors (TLRs) and cytosolic NOD-like receptors (NLRs). The NLRP1 inflammasome is present in motor neurons of the spinal cord as well as in brain cortical neurons. The NLPR2 inflammasome is present in astrocytes and neurons also express the AIM2 inflammasome (De Rivero Vaccari et al., 2016). The NLRP3 inflammasome is primarily expressed in microglial cells (Edye et al., 2014) but also in astrocytes, neurons and endothelial cells (Zhou et al., 2016). Formation of the NLRP3 inflammasome upon activation by PAMPs or endogenous danger signals causes the activation of Caspase-1, which can then cleave the precursor of the pro-inflammatory cytokine IL-1β (pro-IL-1β) into its biologically active form (IL-1β).

The NLRP3 inflammasome consists of the apoptosis-associated speck-like (ASC) adapter protein, which connects the NLRP3 with the downstream effector enzyme (proCaspase-1) (Zhou et al., 2016). Although the NLRP3 inflammasome is the best characterized, a lot more needs to be investigated about the mechanism of its activation. It is unlikely that direct stimulation of NLRP3 by pathogens or specific ligands triggers the inflammasome because the numerous activating compounds have diverse molecular structures (Schroder and Tschopp, 2010).

In the last few years, the contribution of innate immunity to neurological diseases has gathered more attention, especially with the recognition of inflammasome activation (Ramaswamy et al., 2013). The role of inflammasomes in the healthy CNS and CNS diseases has achieved substantial recognition in several animal models of neurological conditions (Walsh et al., 2014). For example, NLRP3 has been shown to be expressed in different kinds of diseases such as traumatic brain injury, stroke, brain tumor, neurodegenerative disease, and others (Zhou et al., 2016) and the concentration of one or more inflammasome proteins in biological samples may specify the severity of CNS injury in patients (Jha et al., 2015). Inflammasome activation, with the release of inflammatory mediator, may play a crucial role

in the development of epilepsy after brain injury (Edye et al., 2014). In the case of RE, Ramaswamy et al. revealed a concurrent induction of inflammasome components in both white matter and cortex, disclosing that microglia and macrophages are the chief cells demonstrating inflammasome cellular machinery. Both NLRP1 and NLRP3 presented enhanced expression in brains from RE brain patients compared to controls. More in detail, NLRP1, NLRP3, NLRC4, Caspase-1 and ASC transcripts were consistently detectable in microglia. Only NLRP1 was also expressed in human astrocytes but at low levels and the remaining genes were minimally detected in astrocytes and neurons (Figure 4) (Ramaswamy et al., 2013).

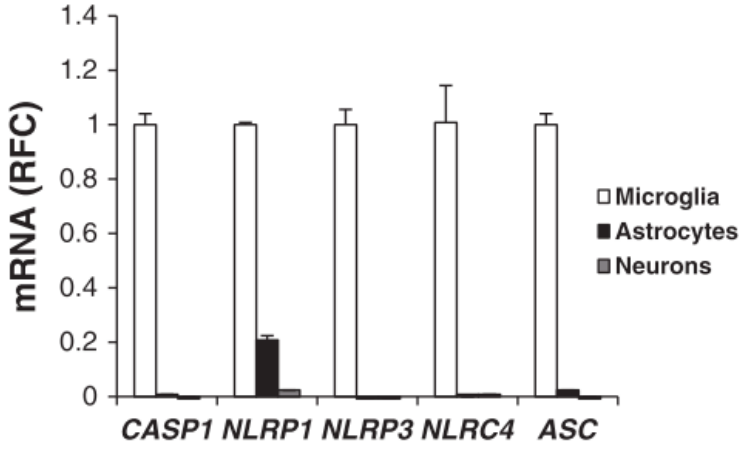

Figure 4. Inflammasome expression in primary human neural cells*. Immunegene transcript levels in primary human microglia, astrocytes and neurons showing that microglia express all inflammasome-associated genes examined unlike astrocytes or neurons* (Ramaswamy et al., 2013).

As the inflammasome complex mediates the release of IL-1β and IL-18 (both of which can trigger a cascade of secondary inflammatory events in neuroinflammation), it represents a potential critical mediator of neuroinflammation and a potential therapeutic target of neurodegenerative disorders including epilepsy (Freeman and Ting, 2016).

3.3 Interleukin-1β in the CNS: pro-inflammatory cytokine and convulsive agent

Interleukin-1β is a potent pro-inflammatory cytokine that functions in the generation of local and systemic responses to infection, injury and immunological challenges, and it is the primary cause of chronic and acute inflammation (Martinon et al., 2002). In the CNS, IL-1β can be produced by a variety of cell types including microglia, astrocytes, endothelial

cells, neurons, and peripheral leukocytes upon infiltrating into the brain (Webster et al., 2017). It is produced as an inactive cytoplasmic precursor (proIL-1β, 35kDa) that must be cleaved at Asp116 to generate the mature active form (IL-1β, 17kDa) (Martinon et al., 2002).

The synthesis, processing and release of IL-1β are tightly controlled in macrophages and microglia. The process requires two signals: the priming signal is mediated by TLRs that activate nuclear factor κB (NF-κB) and mitogen-activated protein (MAP) kinase (MAPK) to induce gene transcription and accumulation of intracellular stores of pro-IL-1β. Nevertheless, the molecular mechanisms regulating the transcription of pro-IL-1β are still being elucidated. In the presence of a second stimulus such as adenosine triphosphate (ATP), induction of inflammasome activation takes place and Caspase-1 is activated enzymatically to process pro-IL-1β to the mature and releasable IL-1β form (17kDa) (Figure 5) (Bryant and Fitzgerald, 2009; Netea et al., 2010; Teresa Ravizza et al., 2006).

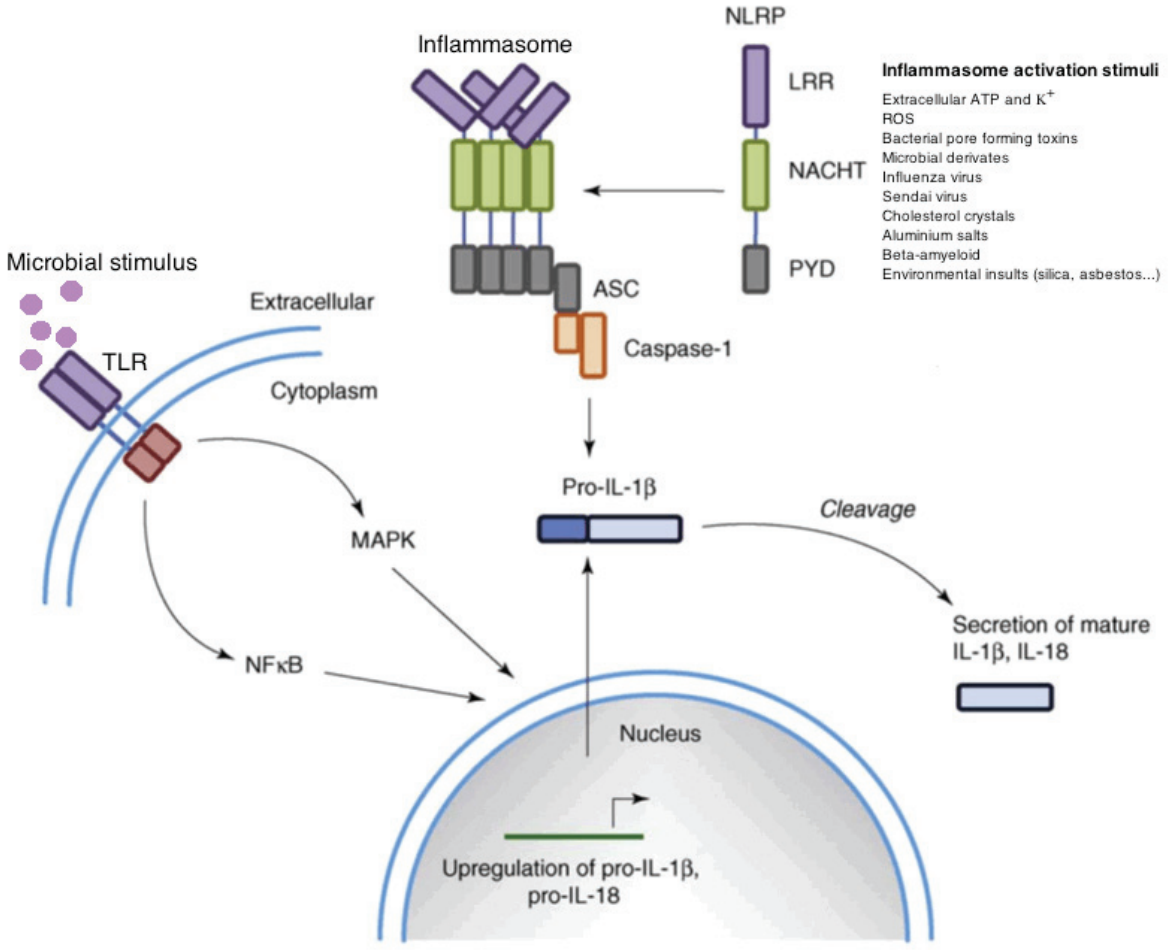

Figure 5. Mechanisms regulating IL-1β production. *Generation of IL-1β requires a priming signal, often from PRRs such as TLRs that activates NF-κB and MAPK pathways that lead to transcription of pro-IL-1β. The pro-IL-1β is then cleaved into the active, mature 17kDa cytokine by Caspase-1. NLR containing inflammasomes activate Caspase-1. Inflammasome oligamerizes upon activation and*

recruit the adapter molecules ASC that subsequently recruits and activates Caspase-1 (*Picture modified from* (Bryant and Fitzgerald, 2009).

IL-1β is known to cause the proliferation of macrophages and neuroinflammatory cells such as microglia and astrocytes. These cells are recruited to the site of injury or inflammation within the CNS and the activation of IL-1β/IL-1R1 triggers the initiation of intracellular signaling pathways such as NFκB and MAPK, which are linked to the transcriptional induction of pro-inflammatory genes and the production of neurotoxic molecules (Vezzani, 2015; Webster et al., 2017). This represents one of the initial signature events during neuroinflammation and a hallmark of pathogenesis associated with various neurodegenerative diseases. Regulation of IL-1β may play a role in attenuating or balancing the innate immune response during neuroinflammation (Freeman and Ting, 2016).

The pro-epileptic actions of IL-1β via IL-1R1 activation occur during the process of epileptogenesis, regardless of whether excitotoxicity and cell death take place or not (Figure 6). IL-1β/IL-1R1 triggers rapid effects on neuronal excitability resulting in ion channel changes mediated by activation of kinases (Src and PI3K). These actions seem to be responsible for the proconvulsive actions of IL-1β and may contribute to seizure-associated neuronal death. However, there is evidence that induction of neuronal cell death does not seem to be a prerequisite for the pro-epileptogenic actions of IL-1β. IL-1β may trigger also long-term effects via transcriptional activation of NFκB and MAPK-dependent genes involved in structural and functional changes in glia and neuronal network. Both actions, separately or together, may contribute to epileptogenesis (Figure 6) (Vezzani and Baram, 2007).

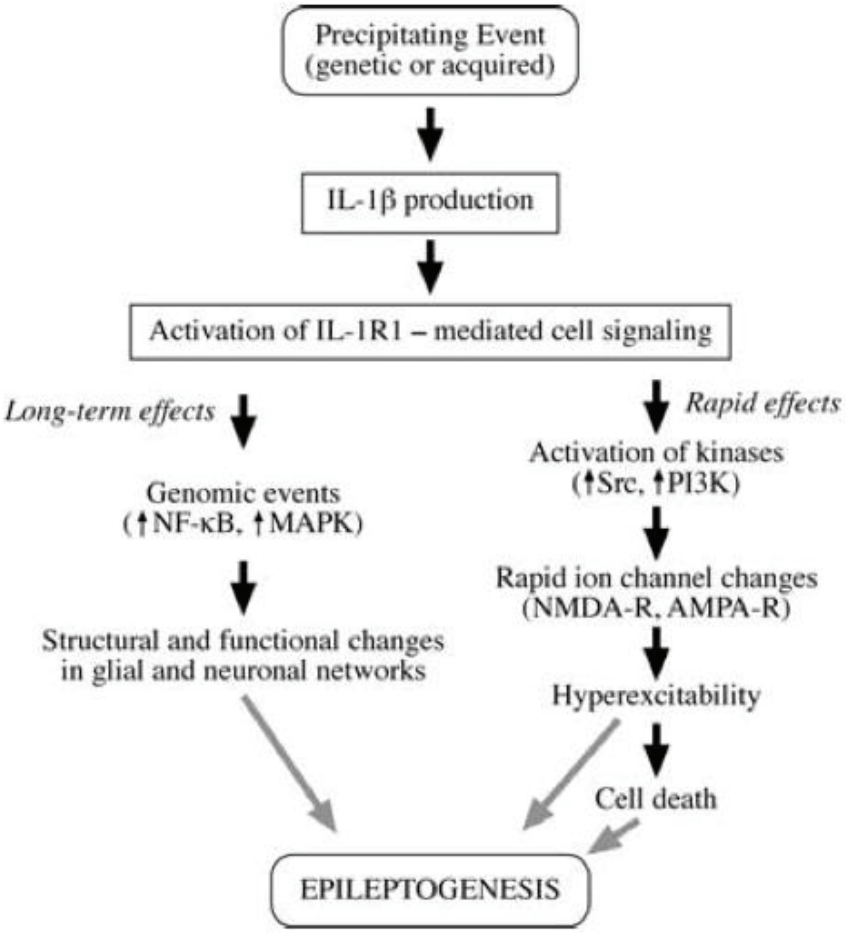

Figure 6. IL-1β and Epileptogenesis. *This schema depicts the cascade of events that may underlie CNS actions of IL-1β after its production and release following a precipitation event. NFκB: nuclear factor kappa B; NMDA-R: N-methyl-D-aspartate receptor; MAPK: mitogen-activated protein kinase; PI3K: phosphatidylinositol-4,5-bisphosphate 3-kinase* (Vezzani and Baram, 2007).

Experimental evidences also support a role for inflammatory processes in the precipitation and recurrence of seizures and neuronal damage (Meng et al., 2014). The involvement of proinflammatory cytokine IL-1β in the development of seizures is supported by pharmacological and genetic studies in animal models, showing that interference with IL-1β reduces the incidence of status epilepticus or attenuates recurrent seizures, whereas its amplification exacerbates seizures as well as lowers the seizure threshold (Meng et al., 2014). Pharmacological blockade or generic inactivation/inhibition of the machinery responsible for IL-1β biosynthesis and release, drastically reduce intrinsic seizure susceptibility in mice (Vezzani, 2015). Vezzani at al. also showed that by providing kainate to rats in order to induce electroencephalographic seizures, microglia were stimulated and produced IL-1β and the cytokine enhanced the induced seizures and tributed to neuronal loss. Moreover, it was found that exogenously applied human recombinant IL-1β enhanced electroencephalographic

seizure activity induced by kainic acid in a dose-dependent and receptor-mediated manner (Vezzani et al., 1999). Furthermore, two rat models of temporal lobe epilepsy have shown that pharmacological blockade of the IL-1β/IL-1R1 axis during epileptogenesis provides neuroprotection (Matin et al., 2015). In humans, elevated IL-1β and IL-1R1 have been detected in brain tissue from patients with temporal lobe epilepsy and IL-1β was also elevated in cerebrospinal fluid from children with febrile seizures. In addition, increased values of IL-1β and inflammasome components have also been observed in other seizures disorders like RE (Edye et al., 2014). IL-1β could also affect neuronal excitability at different levels and it has been shown to participate in neuronal death, perhaps in part via enhanced excitability. Excitatory effects of IL-1β has been reported in various brain regions, in particular, IL-1β reduces synaptically-mediated GABA inhibition in area CA3 of the hippocampus via still unidentified kinases and increases CA1 neuron excitability by reducing N-methyl-D-aspartate (NMDA) channel (Vezzani et al., 2012).

The range of mechanisms by which IL-1β may contribute to epilepsy is increasing with the use of improved research tools. Nevertheless, further investigation in experimental models of acquired epilepsies is needed. For instance, blocking endogenous IL-1β production and/or its cell signaling after an inciting event will aid in gaining a better understanding of the role and relevance of this cytokine in epileptogenesis (Vezzani and Baram, 2007).

3.4 Rasmussen's encephalitis

Rasmussen's encephalitis (RE) is a progressive disease characterized by drug-resistant focal epilepsy, progressive hemiplegia, and cognitive decline, with unihemispheric brain atrophy. The chronic disorder is rare and affects mainly children and young adults (Varadkar et al., 2014). Histopathological hallmarks of RE are cortical inflammation, T cell infiltrates, microglial activation, and microglial nodules, followed by neuronal loss and astrogliosis (Varadkar et al., 2014).

The underlying etiology of RE remains unknown although the inflammation in the brain seems to be driven by an antigen. Several foreign infectious agent have been postulated as causative but autoimmune mechanisms have been also reported (Takei et al., 2010; Varadkar et al., 2014), mainly supported by the infiltration of CD8-positive T lymphocytes and microglia, gliosis and neurodegeneration in the cerebral cortex (Ramaswamy et al., 2013).

Brain tissue from patients with RE has been tested for the presence of several viruses, including Epstein-Barr virus, cytomegalovirus, herpes simplex virus, and enterovirus. None of these studies was able to show a causal association between RE and a specific virus. Finding a rare virus would be much more difficult because methods are limited. Furthermore, infected cells under cytotoxic T-cell attack can be injured and later phagocyted by microglia and

macrophages, thus the chances of finding a virus most likely might happen in the early stage of the disease when surgical sampling is less frequent. Therefore, it will be challenging to search for a RE's pathogen, especially if it is a rare one (Varadkar et al., 2014).

For a long time, it has been the perception that an antibody-mediated immune response is involved in the pathology of RE. In the 1990s, studies showed that antibodies against the ionotropic glutamate receptor subunit 3 (GluR3) were present in serum of RE patients and were responsible for neuronal damage. Further studies suggested that such antibodies not only killed neurons via an antibody or complement-mediated attack but also via direct activation of the ion channel receptors. Later, it became clear that anti-GluR3 antibodies were not present in all RE patients and were not specific for RE because they could be found also in other forms of epilepsy (Bauer and Bien, 2009). Antibodies against other antigens, such as the alpha-7 nicotinic acetylcholine receptor or Munc-18-1, were also identified in sera from a few patients with RE. However, none of the autoantibodies have been found in more than a small number of patients with RE, and responses to plasma exchange are unpredictable therefore, the role of CNS autoantibodies in the pathogenesis of RE is still unclear (Varadkar et al., 2014).

In addition, there are two more immunopathological mechanisms recognized to have a role in CNS degeneration: T-cell cytotoxicity and microglia-induced degeneration (Varadkar et al., 2014). Cytotoxic CD8-positive T lymphocytes seem to play a major part in the pathogenesis of RE and about 10% of the T cells are granzyme B-positive cytotoxic T lymphocytes (Bien et al., 2002; Thompson and Tsirka, 2017). Immunohistochemical evaluation of RE brain specimens revealed that CD8-positive T cells were partially responsible for neuronal cell death being present close to major histocompatibility complex (MHC) class I-positive neurons and astrocytes. Another study found that peripheral CD8-positive T lymphocyte expansion correlated with disease severity (Schneider-Hohendorf et al., 2016). This finding supports the idea that these T cells expand in the periphery and mount an specific attack against single brain antigens within the CNS (Thompson and Tsirka, 2017). Another possibility is that, instead of recognizing an autoantigen, these cytotoxic T lymphocytes could recognize foreign antigens from pathogen-infected neurons and astrocytes localized in a focal area of the brain (Varadkar et al., 2014).

Microglia activation is also a well-founded immunopathological mechanism in RE. Banati et al. found widespread microglial activation in the affected hemisphere of RE (Banati et al., 1999). A study of Wirenfeldt et al. showed extensive microglial activation in RE in addition to a variety of microglial morphologies, however there was not significant correlation between CD8-positive T lymphocytes infiltration and activated microglia (Wirenfeldt et al., 2009). Nevertheless, the precise pathogenic role of microglia in RE is not completely understood (Thompson and Tsirka, 2017).

In addition to microglial activation, astrocytes are also activated in RE and the activation pattern follows nearly the progression of cortical damage (Varadkar et al., 2014).

Pardo et al. defined 5 stages based on the pathologic changes in RE (Pardo et al., 2004) (see Table 1).

Table 1. Staging of cortical pathology in Rasmussen encephalitis (Pardo et al., 2004).

TABLE 3. *Staging of cortical pathology in Rasmussen syndrome*

Stages	Stage 0	Stage 1	Stage 2	Stage 3	Stage 4
Definition	Normal cortex	Early stage	Intermediate stage	Late stage	End stage
Cerebral cortex	Normal	Mild focal inflammation and gliosis	Panlaminar cortical inflammation and gliosis	Panlaminar cortical degeneration and gliosis	Panlaminar cortical cavitation and/or gliosis
Neuronal loss	Absent	Minimal, focal	Moderate to severe, multifocal	Severe, panlaminar	Severe, rare neurons
Astrogliosis	Absent	Mild to moderate, focal	Marked, frequently panlaminar, gemistocytes	Marked, panlaminar, gemistocytes	Variable
Microglial activation	Absent	Mild to moderate, focal	Marked, panlaminar	Variable	Variable
T-cell infiltration	Absent	Mild to moderate, few T-lymphocyte clusters and perivascular cuffs	Marked, panlaminar or multifocal, frequent perivascular cuffs	Minimal	Rare

In stage 0 the cerebral cortex did not present neuronal loss and there was absence of reactive astrogliosis, microgliosis or lymphocyte infiltration. Stage 1 or early stage was defined by the presence of discrete lymphocyte infiltration in superficial and deep neuronal layers of the cerebral cortex. Additionally, the coexistent presence of focal astroglial and microglial reactions was demonstrated. No significant neuronal loss was noted in areas with early pathologic changes but infiltration by lymphocytes were located in perineuronal and perivascular regions. In stage 2 or intermediate stage, they found an increase in the magnitude of lymphocytic infiltration (predominantly T-lymphocytes) and the progression of astroglial and microglial reactions from focal to panlaminar distribution. Microglia and astroglia showed an increase in cytoplasmic volume and extension of multipolar processes as sign of their stage of activation. Evidences of neuronal injury were already observed. The stage 3, also called late stage, showed a significant decrease in the neuronal population, both in large focal areas or panlaminar distribution. Microglia and astroglia continued to show activation and different morphology. However, the inflammatory lymphocytic reaction was not overpowering. The brain presented cortical atrophy and neuronal loss. The end stage or stage 4 was characterized by en extensive destruction of the cerebral cortex. Cortical vacuolation or complete panlaminar neuronal dropout and degeneration were found accompanied by residual astrogliosis, however minimal or absent inflammatory changes remained (Pardo et al., 2004).

Treatment possibilities for RE are limited to controlling the seizures with anti-epileptic drugs together with radical neurosurgical interventions (corticectomy or hemispherectomy) associated with major postoperative neurologic deficits including hemiparesis and hemianopsia (Ramaswamy et al., 2013). However, there are several agents believed to be possible candidates for effective RE treatment, including inhibitors of microglia, drugs targeting excitotoxicity and TNF-α blocking antibody (Thompson and Tsirka, 2017). However, it remains unclear whether any inflammatory mediator, e.g. IL-1β, will become a successful anti-epileptic drug target.

4 Aims of this thesis

The neuropathological studies performed until now in Rasmussen encephalitis (RE) demonstrate the multifocality and heterogeneity of pathologic changes in this disorder (Pardo et al., 2004). The components of change include microglia activation and early death of glia and neurons (Varadkar et al., 2014), T-lymphocyte infiltrates and neuroglial reactions as the major inflammatory responses (Pardo et al., 2004). These inflammatory components of the disease suggest important avenues for exploration of potential immunopathogenic mechanisms in RE.

This study aimed to analyze the presence and cell-type localization of the pro-inflammatory cytokine IL-1β, its receptor interleukin 1 receptor 1 (IL-1R1) and Caspase-1 in RE disease. Formalin-fixed paraffin-embedded (FFPE) and cryo tissues were used from human RE patients at different stages of the disease and control group. Additionally, FFPE tissue from Rhesus monkey with Experimental Autoimmune Encephalomyelitis (EAE) was used as positive control. Following the aims of this thesis are presented.

1. **Detection and quantification of IL-1β in RE at protein level.**
   The amount of IL-1β was analyzed by western blot in FFPE RE and Rhesus monkey with EAE. Moreover, analysis of immunohistochemically stained sections was done by light microscopy and manual counting on the microscope was performed in order to quantify the number of IL-1β positive cells in the investigated sections.

2. **Quantification of gene expression of IL-1β and IL-1R1 in RE and control group.**
   Real time qPCR was performed to quantify the transcript level of the cytokine and its receptor in RE and the control group.

3. **Are IL-1β and IL-1R1 differently expressed in RE stages?**
   Data obtained from immunohistochemical stainings and qPCR was analyzed and statistical analysis was done to compare the expression levels of IL-1β and IL-1R1 during the progression of the disease and the control group. We used FFPE samples from RE cases in different stages of the disease and control cases.

4. **Which cells in the CNS express IL-1β, IL-1R1 and Caspase-1?**
   Double and triple confocal fluorescence stainings with markers for astrocytes (GFAP), microglia (Iba-1 and CD68) and neurons (NeuN) were performed to elucidate the localization of IL-1β, its receptor and Caspase-1.

5 Materials and Methods

5.1 Study Samples

In this study formalin-fixed, paraffin-embedded (FFPE) human biopsy brain tissue of patients suffering from Rasmussen encephalitis (RE) (n=14) was used and FFPE human autopsy and biopsy brain tissue controls (C) (n=11) were also used (see Table 2). 13 RE cases and 9 of the controls were provided by the Bethel Epilepsy Center in Bielefeld-Bethel (Germany), sample 1471/97 was from the Department of Epileptology at the University Hospital of Bonn and 2 controls (91/10/4 and 140/05/1) came from Göttingen. An additional fresh frozen RE case (Y146/16/2) was used for confocal microscopy. For Western blot analysis and confocal microscopy a sample (Y318/10/2) from Rhesus Monkey with Experimental Autoimmune Encephalomyelitis (EAE) was used as a positive control.

Patients were from both genders, male (m) and female (f), and the disease was found either in the right (r) or the left (l) brain hemisphere (see Table 2). The age of surgery between the patients was variable. The average age between the controls samples was 28,23 years old being the oldest patient 43,87 years old and the youngest 4,85. For the RE cases, the average age was 8,24 years being the oldest patient 24,58 years old and the youngest 4,83.

The stage of the disease was determined in each patient prior to start with any experiment. Three different groups were defined (stage 1, 2 and 3) based on immunohistochemical (IHC)-staining method using the following markers: CD68 (microglia marker), CD3 (T cells marker) and NeuN (neuronal marker) (see Table 2).

Table 2. Samples of RE and control patients used in the study.

SAMPLE	DISEASE	STAGE of the DISEASE	GENDER	AFFECTED HEMISPHERE	SAMPLE AREA
707/03/d	Control	-	f	l	temporal cortex (tc)
395/99/f	Control	-	m	l	tc
91/10/4	Control	-	m	r	gyrus cinguli right
723/10/5	Control	-	f	l	tc
140/05/1	Control	-	m	l	frontal left
1998/05/I2	Control	-	f	l	tc

805/11/I3	Control	-	f	l	tc
764/10/II3	Control	-	f	l	tc
35/10/10	Control	-	m	r	tc
826/06/b	Control	-	m	l	tc
1181/11/7	Control	-	m	l	tc
247/05/I2	RE	1 & 2	m	r	tc
128/14/I3	RE	1	f	l	tc
61/14/II2	RE	1 & 3	f	r	cortex (CTX) hemispherectomy
912/93/I7	RE	1	f	l	tc
1762/00/I4	RE	1	f	r	frontal CTX
877/12/I2	RE	1, 2 & 3	m	r	insula
1471/97	RE	1	m	unknown	unknown
899/13/I2	RE	2	f	r	tc
127/15/I	RE	2	m	r	amigdala
542/12/IIb	RE	2	f	l	CTX hemispherectomy
1385/92/I6a	RE	2	f	r	frontal CTX
1909/96/I5	RE	2 & 3	m	r	frontal CTX
144/14	RE	3	m	r	tc
1414/91/8b	RE	3	f	l	frontal CTX

5.2 Protein detection - Western Blot

5.2.1 Materials

- 8µm thick FFPE sections placed in Eppendorf tubes.

- Vortex Mixer 7-2020 (neoLab; Ser.-Nr. 000769)
- Analytic scale AB204 (Mettler Toledo; SNR 1115432306)
- Fume hood (SM Labortechnik)
- Centrifuge 5424 (Eppendorf AG; Ref. #0007787)
- 1,5 ml Eppendorf tubes (Biozym; Art.Num. 710340)
- Xylene (Avator Materials; Ref. 3410)
- Ethanol (EtOH) 96%, 70% (Brenntag CEE GmbH; Ref. #442269)
- Extraction buffer: 20mM Tris HCl (pH=8,8); 2% SDS and 200mM Beta-mercaptoethanol.
- Protease inhibitor cocktail tablets: cOmplete Tablets, Mini EASYpack (Roche; Ref. 04 693 124 001)
- Extraction buffer + Protease Inhibitor: 1 tablet of protease inhibitor was dissolved in 10ml of extraction buffer. The dilution was kept at 4°C.
- BD Microlance™ 20Gx1´´ needles (BD; Ref. #304827)
- Bioer Thermocell Cooling&Heating Block (Biozym Scientific GmbH; Model: CHB202)
- Thermomixer compact (Eppendorf AG; Ref. #5350 02509)
- Heidolph Polymax 1040 (Heidolph Instruments; Ref. #543-42210-00-3)
- 10X Running buffer stock solution pH=8,3 (1L): 250mM Tris were mixed with 1900mM Glycine and 1% SDS in 1L of double-distilled water.
    - 1X Running buffer working solution (1L): 100ml of running buffer stock solution were diluted in 900ml of double-distilled water.
- 10% APS: 1g APS was dissolved in 10ml double-distilled H_2O. It was stored at 4°C for few weeks.
- 10X Transfer buffer stock solution pH=8,3 (1L): 250mM Tris and 1900mM Glycine were dissolved in 1L of double-distilled water.
    - 1X Transfer buffer working solution (1L): 100ml of transfer buffer stock solution were diluted in 900ml of double-distilled water. Then 10% MeOH was added and properly mixed.
- 10X TBST stock solution pH=7.5 (1L): 200mM Tris, 150mM NaCl and 1% Tween 20 were dissolved in 1L of double-distilled water. pH needed to be adjusted to 7,5.
    - 1X TBST working solution (1L): 100ml of TBST stock solution were diluted in 900ml of double-distilled water.
- Precision Plus Protein™ WesternC™ Blotting Standards (BIO-RAD Laboratories; Cat. #161-0376).
- 1,0mm cassettes (NOVEX by Life Technologies; Ref. #NC2010)
- Prot/Elec™ Tips, Bulk (BIO-RAD Laboratories; Cat. #223-9915)
- XCell Sure Lock™ Electrophoresis Cell – Novel Mini-Cell (Invitrogen; Serial No. 1263323-3271)
- XCell Sure Lock™ Blotting module (Invitrogen; Serial No. 1263323-3271)
- Electrophoresis power supply EV222 (PEQLAB; Cat. No. 55-EV222)
- Magnetic Stirrer IKAMAG® RH (IKA; Ref. RH226744)

- Ponceau S solution (Sigma-Aldrich; Lot. #SLBN3529V)
- Blocking solution: 5% (w/v) milk powder in 0,1% TBST.
- Amersham™ ECL™ Prime Western Blotting Detection Reagent (GE Healthcare Life Sciences, Product code: RPN2232)
- Molecular Imager® ChemiDoc™ XRS+ (BIO-RAD Laboratories; Article No. 1708265)
- Urea gels

Table 3. 5% Stacking Gel (7ml)

Acrylamide (40%)	0,625ml
0,5M Tris	1,25ml
Urea	1,8g
ddH_2O	fill up to 5ml
10% APS	50µl
TEMED	10µl

Table 4. 11% Running Gel (12ml)

Acrylamide (40%)	2,73ml
1,5M Tris	2,2ml
Urea	3,2g
ddH_2O	fill up to 10ml
10% APS	44µl
TEMED	8,8µl

- Primary antibodies diluted in blocking solution

Table 5. Primary antibodies

Antibody (Ab)	Antibody type	Target	Dilution	Source
ß- actin	Mouse monoclonal Ab	N-terminal of beta isoform of ß-actin	1:10000	Abcam ab6276

Interleukin-1beta (IL-1β)	Goat polyclonal Ab	Human and monkey IL-1β	1:250	Santa Cruz Biotechnology (C-20) #sc1250

- Secondary antibodies diluted in blocking solution

Table 6. Secondary antibodies

Antibody (Ab)	Target	Dilution	Source
donkey-α-goat HRP	IgG (H+L)	1:5000	Jackson ImmunoResearch (#705-035-147)
POX-α-mouse ß-actin	IgG (H+L)	1:10000	Jackson ImmunoResearch (#715-035-151)

5.2.2 Method

Western blot assay was used for the detection and quantification of protein IL-1β in the study cases. The protein extraction protocol was established based on Addis el al. protocol for protein extraction from FFPE tissue (Addis et al., 2009).

Prior to starting with deparaffinization of the tissue, 1,5ml empty Eppendorf tubes were weighed. 3 serial 7µm thick sections were placed in one tube. Deparaffinization steps were done according to Qiagen protocol from Qproteome FFPE Tissue Kit (Cat No./ID: 37623). Next, the samples were washed with 1ml of double-distilled water one time, the tubes were centrifuged at 20.000rcf for 2 minutes and all the supernatant was discarded. For tissue weight determination the weight of the empty tubes were subtracted from the weight of the tube+tissue.

For the protein extraction, extraction buffer mixed with protease inhibitor tablet was added to each tube in a ratio 5:1 (extraction buffer/protease inhibitor: tissue weigh). In some cases where the amount of tissue was very little, 200µl of extraction buffer with protease inhibitor was added. The samples were incubated at 100°C for 20 minutes and then transferred to another incubator at 80°C for 1 hour with shaking. After 1 hour, all the samples were homogenized with a 20G needle and again they were brought back to the incubator at 80°C for another hour and shaking. All the tubes were cooled down and were centrifuged at 12.000g for 15 minutes at 4°C. The supernatants were transferred into new Eppendorf tubes and were stored at -20°C until further use.

Two urea gels were prepared according to the tables above (see Table 3, Table 4) and placed on buffer core. The gels tension wedge was locked and the chamber was filled with running buffer and also the electrode was covered with buffer. A total volume of 20µl was prepared

per sample: 5µl of loading dye were mixed with 7,5µl of Tris HCl and 7,5µl of sample. The mixture was properly vortexed, centrifuged shortly and incubated at 95°C for 5 minutes. The samples were cooled down on ice before loading. 3-5µl of ladder and 10µl of each sample were loaded into the wells for both gels. The running conditions were 55V until the dye reached the running gel and then 120V were applied until the dye reached the bottom of the gel.

For blotting, two PVDF membranes were soaked into pure methanol for 1 minute and rehydrated in transfer buffer. The transfer sandwiches were assembled inside transfer buffer trying to avoid air bubbles. Blotting was performed overnight in transfer buffer at 4°C and 25V with an additional cooling insert and under constant mixing with a magnetic stirrer.

Next day the PVDF membranes were briefly stained with Ponceau S to confirm successful blotting. The membranes were washed with double-distilled water and then blocked with 5% (w/v) milk powder in 0,1% TBST for 2 hours at room temperature on a shaker. The membranes were washed 3 times for 5 minutes with 0,1% TBST and incubated with the primary antibodies (see Table 5) overnight at 4ºC with gentle agitation. On the next day, the membranes were washed 3 times for 5 minutes with 0,1% TBST and incubated with the secondary antibodies (see Table 6) for 2 hours at room temperature with gentle agitation. The membranes was again washed 3 times for 5 minutes with 0,1% TBST. For detection the membranes were incubated for 5 minutes with Amersham™ ECL™ Prime Western Blotting. Molecular Imager® ChemiDoc™ XRS+ with Image Lab 5.1 software was used for detection. Blots were exposed to chemiluminiscence in a range between 2 seconds and 5 minutes for gel imaging.

5.3 Isolation of total RNA from FFPE tissue

5.3.1 Materials

- 8µm FFPE sections (RNAse-free cut) mounted on normal glass slides.
- Fume hood (SM Labortechnik) under RNAse-free conditions.
- Incubator (55°C and 70°C) (Heraeus Instruments – Thermo Electron Corporation)
- High Pure FFPE RNA Micro Kit (Roche, Ref. #04823125001)
- Lysis buffer (per isolation): 60µl tissue lysis buffer were mixed with 10µl of 10%SDS.
- RNase Zap® (LifeTechnologies, AM9780)
- RNase-free H_2O (Gibco, LifeTechnologies, 10977)
- 10% SDS (Alfa Aesar, 1711183)
- RNase-free 1,5 ml Eppendorf tubes
- RNase-free 0,6 ml Eppendorf tubes (Biozym, 710300)
- Xylene (Avator Materials; Ref. 3410)

- Ethanol (EtOH) 96%, 70% (Brenntag CEE GmbH, 442269)
- EtOH absolute (Merck Millipore #64-17-5)
- Surgical disposable scalpels (Braun Aesculap Division #5518091).
- Vortex Mixer 7-2020 (neoLab; Ser.-Nr. 000769)
- Centrifuge 5415D (Eppendorf)
- Centrifuge Sigma 1-14 (Linder Labortechnik)

5.3.2 Method

The whole process for total RNA isolation from FFPE tissue was performed under RNAse free conditions. The equipment and working area were cleaned prior to starting with 96% EtOH and RNase Zap® (LifeTechnologies, AM9780). HE stained section of each sample where used to indicate which region should be isolated. Using a different scalpel per sample, the selected regions were scratched and the material was collected in Eppendorf tubes. The samples were deparaffinized by adding 800µl of xylene, vortexing 3 times for 4 seconds and 2 minutes incubation. The samples were vortexed again 3 times for 4 seconds, followed by 5 minutes incubation. Centrifugation at maximum speed (13.200rpm) for 2 minutes was performed. Xylene was removed from each sample without disturbing the pellet. All steps with xylene were repeated once. Next, 800µl of EtOH absolute were added to each Eppendorf tube. The samples were properly vortexed 3 times for 4 seconds and then they were centrifuged at maximum speed (13.200rpm) for 2 minutes. The ethanol was removed from each Eppendorf without disturbing the pellet. 800µl of 70% EtOH were added in each tube and vortexed 3 times for 4 seconds. The samples were centrifuged at maximum speed (13.200rpm) for 2 minutes and the ethanol was removed after centrifugation without disturbing the pellet. Samples were centrifuged once more at maximum speed (13.200rpm) for 30 seconds to remove EtOH residuals. The samples were air dried for 20-25 minutes in a well-cleaned box in the incubator at 55°C with lid open until all the EtOH was evaporated. When the samples were perfectly dried, 70µl of lysis buffer was added into each Eppendorf. Immediately after 30µl of Proteinase K were added to each sample and it was mixed thoroughly by vortexing for 3-4 seconds. All the tubes were shortly centrifuged and incubated for 10 hours at 55°C in the incubator followed by 20 minutes at 70°C. At this point, the tubes were stored at -80°C until further use.

To continue with the RNA isolation, the samples were thawed and kept on ice, as well as the DNase I. To each samples, 200µl of binding buffer and 200µl of EtOH absolute was added. The tubes were vortexed 3 times for 4 seconds and centrifuged at 8.000x g for 1 minute. Filter tubes and collection tubes provided in the High Pure FFPE RNA Micro Kit (Roche, Ref. #04823125001) were combined and the lysates were pipetted into the upper reservoirs. The tubes were centrifuged at 8000x g for 30 seconds and the flow-through was discarded. Another centrifugation step was done at maximum speed for 1 minute and the remaining flow-through was discarded. 30µl of DNase Solution (3µl of DNase Incubation Buffer and 27µl of DNase I) was prepared and added per sample. Next, the samples were incubated at

room temperature for 15 minutes. 300µl of Wash Buffer I were added per sample followed by centrifugation at 8.000x g for 15 seconds. Flow-through was discarded and 300µl of Wash Buffer II were added in each tube repeating the centrifugation and discarding the flow-through. 200µl of Wash Buffer II was added, the samples were centrifuged at 8.000x g for 15 seconds and the flow-through was discarded. The filter tubes were placed in fresh collection tubes and centrifuged at maximum speed for 2 minutes. Once again the filter tubes were placed in fresh 1,5ml Eppendorf tubes and 20µl of Elution Buffer were added and incubated for 1 minute at room temperature. The tubes were centrifuged at 8.000x g for 1 minute and the eluate was reloaded, again incubated for 1 minute at room temperature and centrifuged at 8.000x g for 1 minute. The centrifugation step was repeated at maximum speed for 2 minutes. The eluates were transferred to new 0,5ml Eppendorf tubes and a 2µl aliquot from each sample was used to analyze the integrity and concentration of the isolated RNA by the Agilent 2100 Bioanalyzer RNA Pico (Agilent Technologies, Inc.; DE20901520). The rest of the RNA was stored at -80°C.

5.4 cDNA synthesis

5.4.1 Materials

- RNA samples
- Fume hood (Holter LaminAir)
- Vortex Mixer 7-2020 (neoLab; Ser.-Nr. 000769)
- MyFuge™ Mini centrifuge (Benchmark Scientific C1008-B*)
- iScript™ cDNA Synthesis Kit (Cat. #170-8891)
- MyCycler™ Thermal Cycle (BIO-RAD Laboratories, Serial No. 580 BR)
- PCR soft tubes 0,2ml DNase/RNase Free (Biozym Biotech Trading GmbH, Art.-Nr. 710908)
- RNase-free 1,5 ml Eppendorf tubes

5.4.1.1 Reaction Setup

Table 7. Reaction setup for cDNA synthesis

Component	Volume per Reaction (µl)
5x iScript reaction mix	4 µl
iScript reverse transcriptase	1 µl
Nuclease-free water	x µl
RNA template (100fg to 1µl total RNA)	x µl

Total volume	20 µl

5.4.2 Method

The whole process for cDNA synthesis was performed under RNAse free conditions. The equipment and working area were cleaned prior to starting with 96% EtOH and RNase Zap® (LifeTechnologies, AM9780).

According to the number of samples, a master mix was made with the 5x iScript reaction mix and the iScript reverse transcriptase (see Table 7) the amount of RNA added was adjusted to a final RNA concentration of 4ng. Nuclease free water was added to for a final volume of 20µl. A negative control was used consisting of 5µl of master mix and 15µl of nuclease free water. The samples were incubated in the thermal cycler at 25°C for 5 minutes followed by 30 minutes incubation at 42°C and the final 5 minutes at 85°C. Samples were stored at 4°C for near future use.

5.5 Real Time Quantitative PCR

5.5.1 Materials

- cDNA samples
- MyFuge™ Mini centrifuge (Benchmark Scientific C1008-B*)
- StepOnePlus Real-Time PCR System (AB Applied Biosystem)
- Vortex Mixer 7-2020 (neoLab; Ser.-Nr. 000769)
- Fume hood (Holter LaminAir)
- SsoAdvanced™ Universal SYBR® Green Supermix (Catalog #172-5271)
- PCR soft tubes 0.2ml DNase/RNase Free (Biozym Biotech Trading GmbH, Art.-Nr. 710908)
- Multiplate® PCR Plates™ 96-wells (BIO-RAD Laboratories, Cat. MLL9601)
- Microseal® ´B´seal Seals (BIO-RAD Laboratories, Cat. MSB1001)
- RNase-free 1.5 ml Eppendorf tubes
- RNase-free H_2O (Gibco, LifeTechnologies, Ref. #10977)

5.5.1.1 Real-Time PCR Primers

Table 8. Human primers design for real-time PCR

Gene		Forward Primer	Reverse Primer
GAPDH	5′ end	5′-ATATTGTTGCCATCAATGACCC-3′	5′-ATGACAAGCTTCCCGTTCTC-3′
GAPDH	3′ end	5′-CATTTCCTGGTATGACAACGA-3′	5′-CTTCCTCTTGTGCTCTTGCT-3′
IL-1ß	3′ end	5′-TACAGCTGGAGAGTGTAGATCC-3′	5′-GGGCAGACTCAAATTCCAGC-3′
IL-1R1	5′ end	5′-AGACAAGGCCTTCTCCAAGA-3′	5′-GTTCCTTGCATTTATCAGCCTC-3′

5.5.1.2 Reaction Setup

Table 9. Reaction setup for real time PCR

Component	Volume per 10µ Reaction	Final Concentration
SsoAdvanced universal SYBR® Green supermix	5µl	1x
Forward primer	0,2µl	200nM
Reverse primer	0,2µl	200nM
Template (cDNA)	1µl	cDNA
Nuclease-free H_2O	3,6µl	-
Total reaction mix volume	10µl	-

5.5.1.3 Thermal Cycling Protocol

Table 10. Thermal cycling protocol for real-time quantitative PCR

Real-Time PCR System	Setting/Mode	Polymerase Activation and DNA Denaturation	Amplification			Melt-Curve Analysis
			Denaturation at 95°C/98°C	Annealing/Extension + Plate Read at 60°C	Cycles	
ABI 7500, StepOne, StepOnePlus, 7900HT and ViiA7	Standard	30sec at 95°C for cDNA	15sec at 95°C	30sec	50	65°C-95°C 0.5°C increment 2-5 sec/step (or use instrument default setting)

5.5.2 Method

Real-time quantitative qPCR was used to quantify the gene expression of IL-1β and IL-1R1 in the control and RE cases. The housekeeping gene GAPDH was used as reference gene to normalize the results. For this study mRNA extracted from FFPE tissue was used, which has a very high degree of degradation, which does not occur equally between the 5' and 3' end. The 3' end tends to be better protected from nucleases due to the poly-A-tail. Moreover, fixation, storage conditions, etc. affect the mRNA quality. To rule out bias due to differential degradation between mRNA ends, the housekeeping gene primers were selected according to the amplification site of the gene of interest. Therefore, IL-1β gene was amplified with 3′ end primers and it was normalized with the GAPDH gene amplified also by using 3′ primers (see Table 8). For the amplification of IL-1R1 gene, 5′ end primers were used and it was normalized with GAPDH gene amplified by using 5′ primers (see Table 8). The reaction mix was prepared by thawing the SsoAdvancedTM universal SYBR® Green supermix and other frozen reaction components like the cDNA samples and the forward and reverse primers. All of them were mixed thoroughly and centrifuged briefly to collect solutions at the bottom of tubes, and then they were stored on ice protected from light. Enough reaction setup for all qPCR reactions was prepared by adding the SsoAdvancedTM universal SYBR® green supermix all and the nuclease-free H_2O (see Table 9) and stored on ice. The assay master mix was properly mixed to ensure homogeneity and equal aliquots were dispensed into 4 RNase-free 1.5ml Eppendorf tubes. The right pair of forward and reverse primers was added in one of the four tubes and the mixture was thoroughly mixed (see Table 9). 9µl of master mix was dispensed into each well of the 96-wells PCR plate. 1µl of template (cDNA) was added in each well. Every sample was loaded in triplicates, as well as the negative controls that contained the master mix and 1µl of nuclease-free H_2O instead of cDNA (see **Table 9**). The 96-wells PCR plate was sealed with an optically transparent film and vortexed for 30 seconds to ensure thorough mixing of the reaction components. The plate was spun down at 4ºC for 2 minutes to remove any air bubbles and collect the reaction mixture in the well bottom. The thermal cycling protocol was programmed according to the manufacturer's recommendation (see Table 10). The qPCR data analysis was performed according to the instrument-specific instructions. The samples were divided in the 4 groups of interest: control, stage 1, stage 2

and stage 3. IL-1β results were normalized with GAPDH-3' results and IL-1R1 data was normalized with GAPDH-5' data. Ct was determined by single threshold at 0,3 in all amplifications. From the triplicate of each sample the average of the Ct value was calculated for each amplified gene. Delta Ct (ΔCt) was calculated by subtracting the average Ct value of GAPDH from the average value of the genes of interest. The average of all ΔCt of control samples was calculated and it was used to define the ΔΔCt. The fold change of gene expression was calculated ($2^{-\Delta\Delta Ct}$) followed by a log-transformation (log10). For statistical analysis GraphPad Prism 6 was also used to process and interpret the data. For comparison of control cases and pooled RE cases unpaired t-test was used and One-Way ANOVA with post-hoc Holm-Sidak's multiple comparisons test was performed to compare control cases and each stage of RE. All graphical data is represented as mean with the standard error of the mean (SEM) and p-values below 0,05 were considered to be significant.

5.6 Immunohistochemistry - ABC System with peroxidase activity for detection

5.6.1 Materials

- 3-5µm thick FFPE sections mounted on normal glass slides
- Xylene (Avator Materials; Ref. 3410)
- Ethanol (EtOH) 96%, 70% and 50% (Brenntag CEE GmbH, Ref. #442269)
- TBS-buffer
    - TBS-stock solution pH 7.5 (1L): 60,57g of 25mM Tris buffer, 180g of 150mM NaCl and 400ml of 1N HCl were dissolved in deionized water (a.d). The pH was adjusted to 7,5 by adding 1N HCl.
    - TBS working solution: the stock solution was diluted 1:20. 50ml of stock buffer were diluted in 950ml of a.d.
- PBS-buffer
    - PBS-stock solution pH 7.4 (2,5L): 13,8g of 0,04M NaH_2PO_4, 71,2g of 0,16M Na_2HPO_4 and 90g of NaCl were dissolved in a.d. The pH was adjusted to 7,4.
    - PBS working solution: the stock solution was diluted 1:4. 250ml of stock solution were diluted in 750ml of a.d.
- H_2O_2/Methanol: 150mL of Methanol and 1ml H_2O_2 (30%) were mixed.
- 10% FCS/DAKO-Buffer: the commercial DAKO-buffer solution from Dako corporation 10x (#S3006) was diluted 1:10 with deionized water. For dilution of primary, secondary antibodies and Avidin Peroxidase a solution with 10% FCS in DAKO-buffer was made.
- EDTA-buffer

  - EDTA 20x stock solution: 1,21g of 10mM Tris-buffer and 0,37g of 1mM EDTA were dissolved in 50ml of a.d. The pH was adjusted to 8,5 or 9,0 depending on fixation of material.
  - EDTA working solution: 2,5ml of stock solution was diluted in 50ml of a.d.
- Peroxidase conjugated Streptavidin 1:500 (Jackson Immunoresearch; #016-030-08)
- DAB (3,3′-Diaminobenzidine): 1ml of DAB (K3467 DAKO®) stock solution was mixed in 50ml of PBS. The mixture was filtered with a paper filter into a jar and 16,5µl of H_2O_2 (Merck Millipore) was added.
- Mayers Hemalaun (Merck #1.09249): Mayer´s Hematoxylin (Merck®)
- HCl-ethanol: 100ml of 70% ethanol was mixed with 0,5ml of concentrated HCl (37%).
- Scott's solution: 2g of $KHCO_3$ and 20g of $MgSO_4$ x $7H_2O$ were dissolved in 1.000ml of H_2O.
- Coverslips (Carl Roth; H8762)
- Eukitt (Kindler; R1339)

- Primary antibodies

Table 11. Primary antibodies

Antibody (Ab)	Antibody type	Target	Pre-treatment	Dilution	Source
Interleukin-1beta (IL-1β)	Goat polyclonal Ab	Human IL-1β Monkey IL-1β	EDTA pH=8.5 (1h steamer)	1:250	Santa Cruz Biotechnology (C-20) #sc1250
Caspase-1	Rabbit polyclonal Ab	Monkey Caspase-1	EDTA pH=9 (1h steamer)	1:5000	Merck Millipore (#06-503-I)

- Secondary antibodies

Table 12. Secondary and biotinylated secondary antibodies

Antibody (Ab)	Target	Dilution	Source
Bi-donkey-α-goat	IgG (H+L)	1:500	Jackson ImmunoResearch (#705-065-147)
Bi-donkey-α-rabbit	IgG (H+L)	1:2000	Jackson ImmunoResearch (#711-065-152)

5.6.2 Method

The FFPE tissue was cut into 3-5µm thick sections. For immunohistochemical staining the samples were deparaffinized two times for 15 minutes in xylene and rinsed twice in 96% ethanol. Next, endogenous peroxidase activity was blocked by 30 minutes incubation in H_2O_2-Methanol. Rehydration was performed by immersing the slides shortly (1min) in 96% ethanol, 70% ethanol, 50% ethanol and a.d. Antigen retrieval was done by heating the slides in EDTA (pH 8,5 or 9) or citrate-buffer (pH 6) in a household food steamer device (MultiGourmet FS20; Braun, Kronberg/Taunus, Germany) for one hour. Depending on the used antibody the appropriate pretreatment solution was chosen (see Table 11). Next, the slides were cooled down to room temperature and were washed 3-5 times with TBS buffer. Afterwards, unspecific background reactions were blocked by incubating the samples with 10% FCS-DAKO buffer for 15-20 minutes in a humid chamber at room temperature. After the blocking step the sections were incubated at 4°C overnight with the primary antibody in the respective dilution (see Table 11) in 10% FCS/DAKO buffer in a humid chamber. On the next day, the slides were rinsed on TBS for 3-5 times by 1h incubation with the biotinylated secondary antibody diluted in 10% FCS/DAKO buffer (see Table 12) at room temperature in a humid chamber. The samples were washed with TBS for 3-5 times followed by 1h incubation time with peroxidase-conjugated streptavidin (1:500) in 10% FCS/DAKO buffer in a humid chamber. Washing step in TBS followed the incubation in peroxidase-conjugated streptavidin. The slides were developed under microscopic control in DAB until the color reaction was satisfactory. The enzymatic reaction was stopped by changing the samples from DAB to deionized H_2O. Counterstaining was done by incubating the slides for 15-20 seconds in Mayer's hematoxylin, washed two times with H_2O and differentiated three times in HCl-ethanol. Next, slides were washed two times in H_2O, incubated 4 minutes in Scott's solution and rinsed with H_2O. Following, dehydration the slides through graded ascending ethanol steps (50%, 70%, 95%, 95% and 95%) ending with n-butyl acetate. At the end the samples were mounted with cover slips using Eukitt® for embedding. Examinations under the microscope were performed the next day when the slides were dry.

5.6.3 Quantitative Analysis from light microscopy staining

Analysis of immunohistochemically stained sections was done by light microscopy. Manual counting on the microscope was performed in order to quantify the number of IL-1β positive cells in the investigated sections. An ocular grid was used and the countings were done using the 10x magnification objective. The area of the grid is $1mm^2$ and the number of positive cells per $1mm^2$ was calculated. For statistical analysis GraphPad Prism 6 was used to process and interpret the data. For comparison of control cases and pooled RE cases Mann-Whitney U-test was used and Kruskal-Wallis test with post-hoc Dunn's multiple comparisons test was used to compare control cases and each stage of RE. All graphical data is represented as median with the interquartile range. In all the cases p-values below 0,05 were considered to be significant.

5.7 Hematoxylin-Eosin (HE) staining

5.7.1 Materials

- 3-5µm thick FFPE sections mounted on normal glass slides.
- Xylene (Avator Materials; Ref. 3410)
- Ethanol (EtOH) 96%, 70% and 50% (Brenntag CEE GmbH, 442269)
- Mayers Hematoxylin (Merck #1.09249)
- HCl-ethanol: 100ml of 70% ethanol was mixed with 0,5ml of concentrated HCl (37%).
- Scott's solution: 2g of $KHCO_3$ and 20g of $MgSO_4$ x $7H_2O$ were dissolved in 1.000ml of H_2O.
- Eosin
    - Eosin stock solution: 10g of Eosin were dissolved in 100ml of a.d. and the solution was maturing some days until it was completely dissolved.
    - Eosin working solution: 2,5ml of Eosin stock solution was diluted with 250ml of a.d. and 12 drops of glacial acidic acid were added.
- Coverslips (Carl Rot; H8762)
- Eukitt (Kindler; R1339)

5.7.2 Method

For HE staining the FFPE samples need to be deparaffinized. Therefore the samples were incubated two times for 15 minutes in xylene to be dewaxed. Next rehydration followed and was performed by descending alcohol steps (~1min) through 96% ethanol, 70% ethanol, 50% ethanol and a.d.

The sections were incubated for 5min in haematoxylin (nuclear stain), washed two times in H_2O and differentiated three times in HCl-ethanol. Next, slides were washed two times in H_2O, incubated 5min in Scott's solution and rinsed with H_2O. Following, 4min incubation in Eosin solution (cytoplasmic stain) was performed and washed in water twice. Then, the slides were dehydrated through graded ascending ethanol steps (50%, 70%, 95%, 95% and 95%) ending with n-butyl acetate.

The slides were mounted with cover slips using Eukitt® for embedding and they were left for drying at room temperature for several hours before further examinations.

5.8 Confocal Laser Fluorescence Microscopy on FFPE Tissue

5.8.1 Materials

- 3-5µm thick FFPE sections mounted on normal glass slides.
- Xylene (Avator Materials; Ref. 3410)
- Ethanol (EtOH) 96%, 70% and 50% (Brenntag CEE GmbH, #442269)
- TBS-buffer
    - TBS-stock solution pH 7.5 (1L): 60,57g of 25mM Tris buffer, 180g of 150mM NaCl and 400ml of 1N HCl were dissolved in deionized water (a.d). The pH was adjusted to 7.5 by adding 1N HCl.
    - TBS working solution: the stock solution was diluted 1:20. 50ml of stock buffer were diluted in 950ml of a.d.
- PBS-buffer
    - PBS-stock solution pH 7.4 (2,5L): 13,8g of 0,04M NaH_2PO_4, 71,2g of 0,16M Na_2HPO_4 and 90g of NaCl were dissolved in a.d. The pH was adjusted to 7.4.
    - PBS working solution: the stock solution was diluted 1:4. 250ml of stock solution were diluted in 750ml of a.d.
- 10% FCS/DAKO-Buffer: the commercial DAKO-buffer solution from Dako corporation 10x (#S3006) was diluted 1:10 with deionized water. For dilution of primary, secondary antibodies and Avidin Peroxidase a solution with 10% FCS in DAKO-buffer was made.
- DAKO REAL™ Antibody Diluent (code S2022)
- EDTA-buffer
    - EDTA 20x stock solution: 1,21g of 10mM Tris-buffer and 0,37g of 1mM EDTA were dissolved in 50ml of a.d. The pH was adjusted to 8.5 or 9.0 depending on fixation of material.
    - EDTA working solution: 2,5ml of stock solution was diluted in 50ml of a.d.
- Citrate-buffer pH 6.0: 2,10g of citric acid is dissolved in 1L at a.d.
- Catalysed signal amplification system (CSA)
    - Biotinylated tyramine stock (CSA-stock): 6ml of borate buffer (pH=8) (Merck®) was mixed with 15ml of sulpho-NHS-LCS-Biotin (Pierce, Illinois, USA) and 4,5mg of tyramine (Sigma-Aldrich®). The mixture was left overnight at room temperature for stirring and after it was filtered and stored in small aliquots at -20°C.
    - CSA working solution: 0,5µl of CSA aliquot (1:2000) and 1µl of H_2O_2 (1:1000) were mixed with 1ml of PBS.
- Streptavidin conjugated Cy2 (1:100) (Jackson ImmunoResearch; #016-220-084)
- Prolong™ Gold Antifade Mountant (Thermo Fisher Scientific P36930)
- Coverslips (Carl Roth; H8762)

- Confocal LEICA SP5 DMI 6000 CS laser scan microscope (Mannheim, Germany)

Table 13. Settings for confocal microscope

Lasers	Excitation Lines (nm)	Emission Peak (nm)	Objective Type	Numerical Aperture	Ref. #
Argon	475	510	63X Oil	63X (1.40-0.60)	HCX PL APO CS (11506188)
DPSS 561	561	570			
HeNe 633	633	670			

- Primary antibodies

Table 14. Primary antibodies

Antibody (Ab)	Type of staining	Antibody type	Target	Pre-treatment	Dilution	Source
Interleukin-1beta (IL-1β)	double	Goat polyclonal Ab	Human and monkey IL-1β	EDTA pH=9 (1h steamer) + CSA (20min. RT)	1:250	Santa Cruz Biotechnology (C-20) #sc1250
	triple				1:75	
Caspase-1	triple with Ab from different species	Rabbit polyclonal Ab	p20 subunit of Caspase-1	EDTA pH=9 (1h steamer)	1:1500	Merck Millipore (#06-503-I)
	triple with Ab from same specie			EDTA pH=8.5 (45 min. steamer) + Citrate (45 min. steamer)		
Iba-1	double	Rabbit polyclonal Ab	Microglia and macrophages	EDTA pH=9 (1h steamer)	1:750	Wako Pure Chemical Industries (#019-19741)
	triple			EDTA pH=8.5 (45min. steamer) + CSA (20min. RT) + Citrate (45min. steamer)	1:30000	
GFAP	triple with Ab from different species	Mouse monoclonal Ab	Glial fibrillary acidic protein	EDTA pH=9 (1h steamer)	1:100	Neomarkers MS1376-P1
	triple with Ab from same			EDTA pH=8.5 (45 min. steamer) + Citrate (45 min.		

	specie			steamer)		

- Secondary antibodies

Table 15. Secondary antibodies

Antibody (Ab)	Target	Dilution	Source
Bi-donkey-α-goat	IgG (H+L)	1:500	Jackson ImmunoResearch (#705-065-147)
Bi-donkey-α-rabbit	IgG (H+L)	1:2000	Jackson ImmunoResearch (#711-065-152)
Cy3 donkey-α-rabbit	IgG (H+L)	1:200	Jackson ImmunoResearch (#711-165-152)
Dylight649 horse-α-mouse	IgG (H+L)	1:100	Vector (#DI-2649)

5.8.2 Method for double and triple labeling with antibodies from different species

The FFPE tissue was cut into 3-5µm thick sections. For fluorescence microscopy the samples were deparaffinized two times for 15 minutes in xylene and rinsed in two changes of 96% ethanol. Rehydration was performed by immersed the slides shortly (1min) in 96% ethanol, 70% ethanol, 50% ethanol and a.d. Antigen retrieval was done by heating the slides in EDTA (pH= 9) in a household food steamer device (MultiGourmet FS20; Braun, Kronberg/Taunus, Germany) for one hour. Next, the slides were cooled down to room temperature and were washed 3-5 times with TBS buffer. Afterwards, unspecific background reactions were blocked by incubating the samples with DAKO diluent for 20 minutes in a humid chamber at room temperature. After blocking the sections were incubated at 4°C overnight with the two or the three primary antibodies simultaneously (see Table 14) in DAKO diluent in a humid chamber. On the next day, the slides were rinsed on TBS for 3-5 times and after they were incubated with a biotinylated secondary antibody and one or two fluorescence conjugated secondary antibodies diluted in 10% FCS/DAKO buffer (see Table 15) for one hour at room temperature in a humid chamber protected from light. The samples were washed with TBS for 3-5 times followed by one hour incubation with peroxidase-conjugated streptavidin (1:500) in 10% FCS/DAKO buffer in a humid chamber protected from the light, followed by washing step in TBS. The staining was continued with a signal enhancement step with biotinylated

tyramine. The slides were incubated for 20 minutes at room temperature in CSA working solution followed by washing 3-5 times in TBS. Streptavidin conjugated Cy2 in 10% FCS/DAKO buffer was added to the samples and incubated for one hour at room temperature in a humid chamber protected from light. At the end the slides were washed with deionized H_2O and were mounted with cover slips using Prolong™ Gold Antifade Mountant for protecting fluorescent dyes from fading (photo bleaching) during fluorescence microscopy experiments. Fluorescent preparations were examined using the confocal LEICA SP5 DMI 6000 CS laser scan microscope according to the settings above (see Table 13).

5.8.3 Method for triple labeling with antibodies from the same species

The FFPE tissue was cut into 3-5µm thick sections. For fluorescence microscopy the samples were deparaffinized two times for 15 minutes in xylene and rinsed in two changes of 96% ethanol. Rehydration was performed by immersed the slides shortly (1min) in 96% ethanol, 70% ethanol, 50% ethanol and a.d.. Antigen retrieval was done by heating the slides in EDTA (pH=8,5) in a household food steamer device (MultiGourmet FS20; Braun, Kronberg/Taunus, Germany) for 45 minutes. Next, the slides were cooled down to room temperature and were washed 3-5 times with TBS buffer. Afterwards, unspecific background reactions were blocked by incubating the samples with DAKO diluent for 20 minutes in a humid chamber at room temperature. After blocking the sections were incubated at 4°C overnight with one of the primary antibodies with common origin (see Table 14) in DAKO diluent in a humid chamber. On the next day, the slides were rinsed on TBS for 3-5 times and after they were incubated with a biotinylated secondary antibody in 10% FCS/DAKO buffer (see Table 15) for one hour at room temperature in a humid chamber protected from light. The samples were washed with TBS for 3-5 times followed by one hour incubation time with peroxidase-conjugated streptavidin (1:500) in 10% FCS/DAKO buffer in a humid chamber protected from light, followed by washing step in TBS. The staining was continued with a signal enhancement step with biotinylated tyramine. The slides were incubated for 20 minutes at room temperature in CSA working solution followed by washing 3-5 times in TBS. Antigen retrieval was done by heating the slides in citrate (pH=6) in a household food steamer device (MultiGourmet FS20; Braun, Kronberg/Taunus, Germany) for 45 minutes. Streptavidin conjugated Cy2 in 10% FCS/DAKO buffer was added to the samples and incubated for one hour at room temperature in a humid chamber protected from light, followed by washing 3-5 times in TBS. The sections were incubated at 4°C overnight with the other two primary antibodies simultaneously (see Table 14) in DAKO diluent in a humid chamber protected from light. On the third day, the samples are washed 3-5 times in TBS and incubated with two fluorescence conjugated secondary antibodies diluted in 10% FCS/DAKO buffer (see Table 15) for one hour at room temperature in a humid chamber protected from light. At the end the slides were washed with deionized H_2O and were mounted with cover slips using Prolong™ Gold Antifade Mountant for protecting fluorescent dyes from fading (photo bleaching) during

fluorescence microscopy experiments. Fluorescent preparations were examined using the confocal LEICA SP5 DMI 6000 CS laser scan microscope according to the settings above (see Table 13).

5.9 Confocal Laser Fluorescence Microscopy on Fresh Frozen Tissue

5.9.1 Materials

- 10µm sections of fresh frozen tissue mounted on normal glass slides
- Acetone (VWR Chemicals; Cat. No. 20066.330)
- H_2O_2 30% (Merck Millipore; Cat. 822287)
- TBS-buffer
    - TBS-stock solution pH 7.5 (1L): 60,57g of 25mM Tris buffer, 180g of 150mM NaCl and 400ml of 1N HCl were dissolved in deionized water (a.d). The pH was adjusted to 7.5 by adding 1N HCl.
    - TBS working solution: the stock solution was diluted 1:20. 50ml of stock buffer were diluted in 950ml of a.d.
- 10% FCS/DAKO-Buffer: the commercial DAKO-buffer solution from Dako corporation 10x (#S3006) was diluted 1:10 with deionized water. For dilution of primary, secondary antibodies and Avidin Peroxidase a solution with 10% FCS in DAKO-buffer was made.
- DAKO REAL™ Antibody Diluent (code S2022)
- DAPI (Sigma-Aldrich®): the comercial DAPI fluorescence dye was diluted 1:10000 in PBS.
- TOPRO3 (Invitrogen #T3605): the commercial TOPRO3 fluorescence dye was diluted 1:1000 in PBS.
- Streptavidin conjugated Cy2 (1:100) (Jackson ImmunoResearch; #016-220-084)
- Prolong™ Gold Antifade Mountant (Thermo Fisher Scientific P36930)
- Coverslips (Carl Roth; H8762)

- Primary antibodies

Table 16. Primary antibodies

Antibody (Ab)	Antibody type	Target	Dilution	Source
Interleukin-1beta receptor 1 (IL-1R1)	Rabbit polyclonal Ab	IL-1R1	1:150	Abcam ab106278
GFAP	Goat polyclonal Ab	Glial fibrillary acidic protein	1:100	Santa Cruz Biotechnology (C-19) #sc6170
CD68	Mouse monoclonal Ab	Microglia and macrophages	1:50	Dako Aligent M0814
Neu-N	Mouse monoclonal Ab	DNA-binding neuron-specific protein NeuN	1:500	Chemicon MAB377

- Secondary antibodies

Table 17. Secondary antibodies

Antibody (Ab)	Target	Dilution	Source
Bi-donkey-α-mouse	IgG (H+L)	1:1500	Jackson ImmunoResearch (#705-065-150)
Cy3 donkey-α-rabbit	IgG (H+L)	1:200	Jackson ImmunoResearch (#711-165-152)
Cy5 donkey-α-goat	IgG (H+L)	1:100	Jackson ImmunoResearch (#705-175-147)

5.9.2 Method

The fresh frozen tissue was cut into 10µm thick sections and stored at -20°C. First, the slides were taken out from the -20°C storage and were let air dry at room temperature for at least 30 minutes. Next, the slides were fixed with 40ml acetone and 123µl of H_2O_2 for 10 minutes at 4°C and then they were dried for 20 minutes at room temperature. The samples were washed 3-5 times in TBS. Unspecific background reactions were blocked by incubating the samples with DAKO diluent for 20 minutes in a humid chamber at room temperature. After blocking the sections were incubated at 4°C overnight with the primary antibodies (see Table 16) simultaneously in DAKO diluent. On the next day, the slides were washed 3-5 times in TBS and then they were incubated with biotinylated secondary antibody and fluorescence conjugated secondary antibodies diluted in 10% FCS/DAKO (see Table 17) buffer for one hour at room temperature in a humid chamber protected from the light. Washing 3-5 times with TBS was done next and after the slides were incubated with streptavidin conjugated Cy2 (1:100) for one hour at room temperature in a humid chamber protected from the light. The samples were washed 3-5 times in TBS and were incubated with DAPI (1:500) for 5 minutes at room temperature in an opaque humid chamber. In case the staining was for IL-1R1, the samples were washed 3-5 times in TBS and were incubated 30 minutes with 1M HCl in an opaque humid chamber at room temperature. After, they were washed 3-5 times in TBS and were incubated with TOPRO3 (1:1000) for 15 minutes at room temperature in an opaque humid chamber. At the end the slides were washed with deionized H_2O and were mounted with cover slips using Prolong™ Gold Antifade Mountant for protecting fluorescent dyes from fading (photo bleaching) during fluorescence microscopy experiments. Fluorescent preparations were examined using the confocal LEICA SP5 DMI 6000 CS laser scan microscope according to the settings above (see Table 13).

6 Results

6.1 Detection and quantification of cytokine IL-1β by Western Blot in Rhesus Monkey with EAE and Rasmussen Encephalitis

One of the goals of the project was to detect and quantify by western blot the amount of cytokine IL-1β from FFPE tissue from RE patients. For the establishment of the protocol, samples with a high amount of IL-1β were selected, based on the number of IL-1β positive cells in light microscopy staining. Two RE subjects and one Rhesus monkey with EAE (Figure 7) were finally chosen.

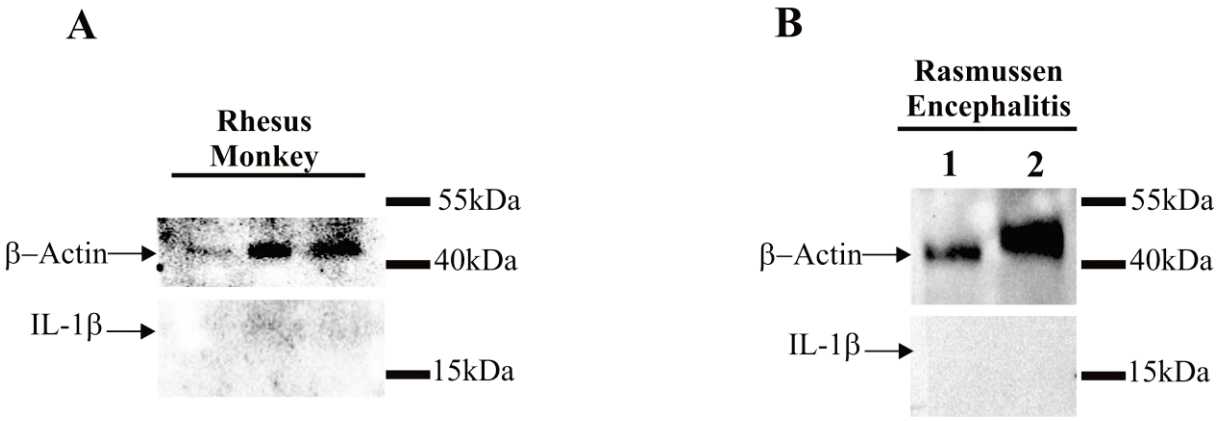

Figure 7. Western blots of IL-1β cytokine expression in Rhesus monkey with EAE and Rasmussen encephalitis. *(A) Blot of Rhesus monkey sample presents β-actin bands around 42kDa in the three wells where sample was loaded but no bands for IL-1β around 17kDa were detected. (B) Blot of RE samples. Case 1 and 2 present β-actin bands around 42kDa but absence of bands for IL-1β around 17kDA. β–actin blots are shown for control of protein loading.*

In order to control the protein loading, the housekeeping gene β-actin was used. Its expression is constant and its molecular weight is far from the molecular weight of IL-1β, allowing for better differentiation of the bands. Both, the samples from Rhesus monkey (Figure 7A) and RE (Figure 7B), presented a band at 42kDa that corresponds with the protein β-actin. The amount of IL-1β was much higher in the monkey, as observed in light microscopy; however, no band was detected in any of the samples at 17kDa (Figure 7).

Although successful establishment of western blot from FFPE tissue was accomplished, as seen by β–actin, quantification of IL-1β was not detectable.

6.2 Analysis of IL-1β and its receptor IL-1R1 by quantitative real time PCR in Rasmussen Encephalitis

The second approach of the project was the quantification of IL-1β and IL-1R1 at the mRNA level in the control group as well as in the different stages of RE. RNA was isolated from the FFPE samples as described in materials and methods section. Next, a quality control check-up of the isolated RNA was done for each sample with the Agilent 2100 Bioanalyzer RNA Pico (Agilent Technologies). Bioanalyzer determines the quantity and quality of the RNA samples and the Pico assay can be used to assay RNA integrity in the 50pg/µl to 5ng/µl range. The analyzer measures the RNA integrity, which is displayed as the RNA Integrity Number (RIN) but it also measures the RNA area, RNA concentration, rRNA ratio (28S/18S) (Figure 8).

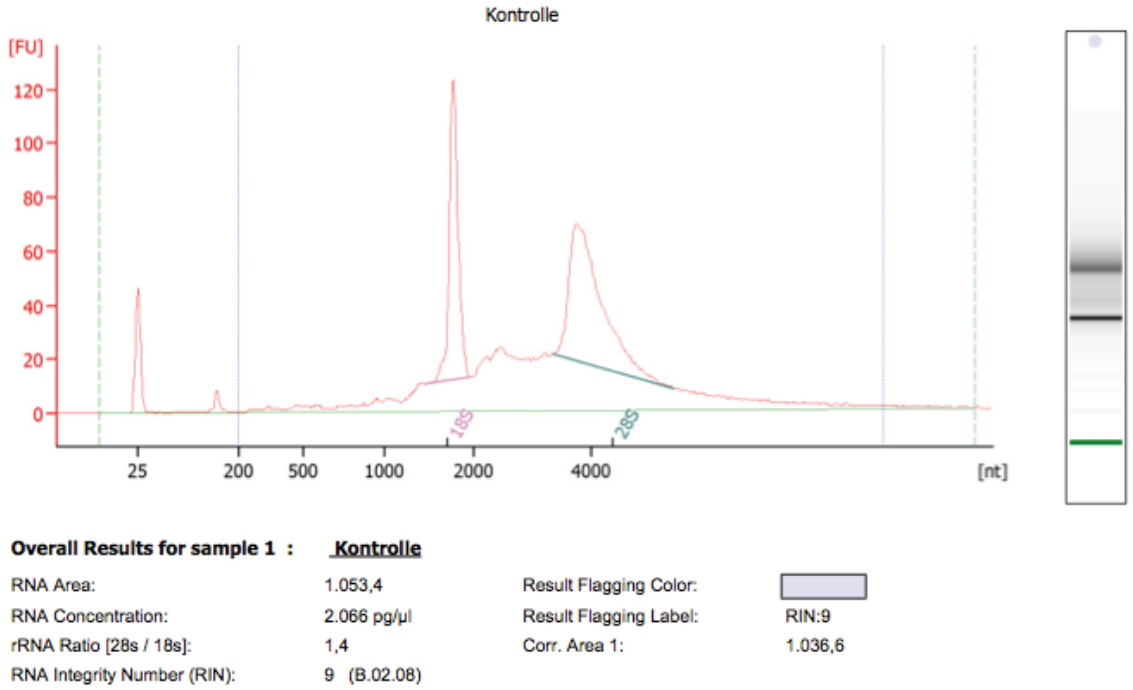

Figure 8. Electropherogram of high-quality control RNA (by Agilent 2100 Bioanalyzer RNA Pico). *The first peak corresponds to the marker peak. Depending on the RNA extraction method, a second peak appears between the marker peak and the 200 nucleotide region. Two ribosomal peaks, the 18S and the 28S rRNA peaks. The baseline region between the internal marker and the 18S rRNA is relatively flat and free of small rounded peaks corresponding to smaller RNA molecules that are degradation products of the rRNA transcripts. FU: fluorescence units; nt: nucleotides.*

A good quality RNA, for example from cell culture samples, has a 28S/18S ratio of two or close to two, as well as the RIN value close to 10 in a scale that ranges from 0 to 10, with 10 indicating maximum RNA integrity.

Electropherograms of RNA isolated from FFPE tissue have to be evaluated differently (Figure 9). This RNA presents an alter curve profile due to a high number of short fragmented RNA pieces. The 28S/18S ratio and the RIN value are very low and cannot be used as criteria for total RNA quality (Figure 9). Therefore, the amplitude and the length of the resulting plateau, as well as the RNA concentration, are used to determine the RNA quality. DV200 value is also considered and it indicates the percentage of RNA fragments per sample with a length over 200 nucleotides. A DV200 of above 70% is considered as high quality RNA. For successful qPCR, sufficiently long RNA fragments are needed and RNA concentration values above 500 pg/µl were selected.

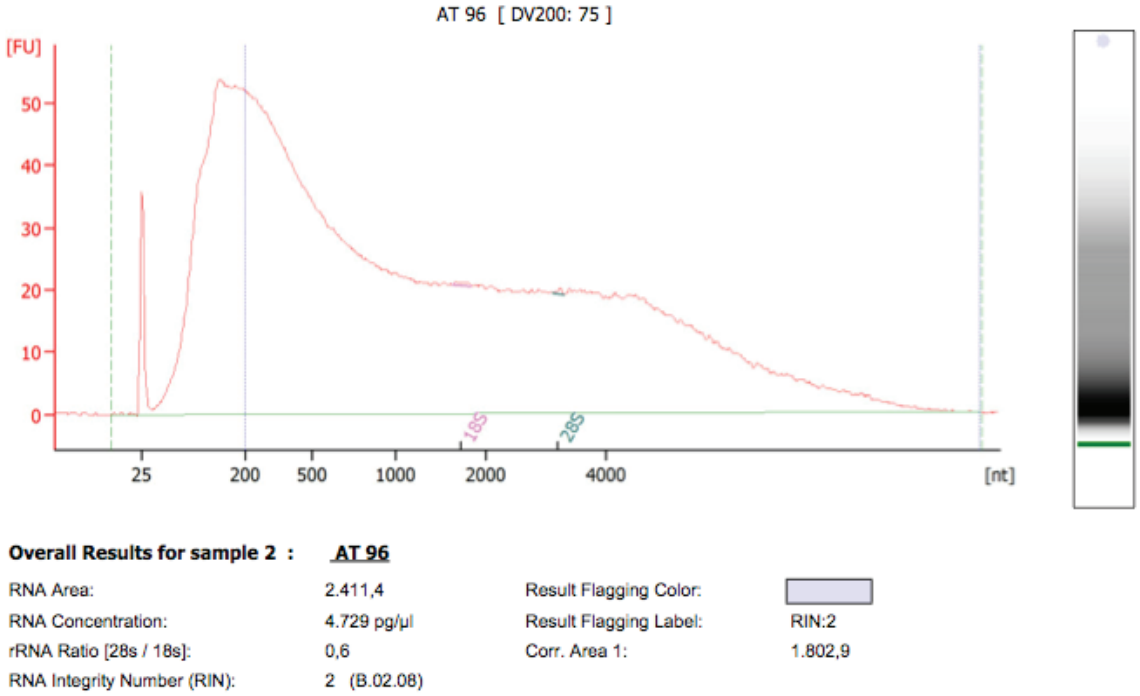

Figure 9. Electropherogram of RNA isolated from FFPE tissue (by Agilent 2100 Bioanalyzer RNA Pico). *The first peak corresponds to the marker peak. Big peak around 200 nucleotides. Two ribosomal peaks, the 18S and the 28S rRNA peaks are not visible. The baseline region between the internal marker and the 18S rRNA is nonexistent. Early drop of the plateau after the peak around 200 nucleotides means a low number of long RNA fragments FU: fluorescence units; nt: nucleotides*

The SYBR® Green quantitative PCR was performed with 4ng of isolated RNA that was previously transcribed into cDNA. All the samples were tested for the genes of interest (IL-1β and IL-1R1) and for the reference gene GAPDH, prior checking that the housekeeping gene was stably expressed in all samples. Water controls were employed as negative control and to exclude the possibility of primer dimer formation.

Firstly, concentration of IL-1β mRNA was studied and all the RE stages were pooled in one group and it was compared to the control group (Figure 10). The unpaired t-test revealed that

the values obtained from the RE group were significantly higher than the ones from control (Figure 10A). Furthermore, the RE stages were analyzed individually and each of them was compared to the control group (Figure 10B). In this case, One-Way ANOVA with post-hoc Holm-Sidak's multiple comparisons test confirmed that every stage presented significantly higher values compared to the control. The line of the graph (Figure 10B) slightly rose at stage 3, although the statistical analyses did not show significant differences between RE stages.

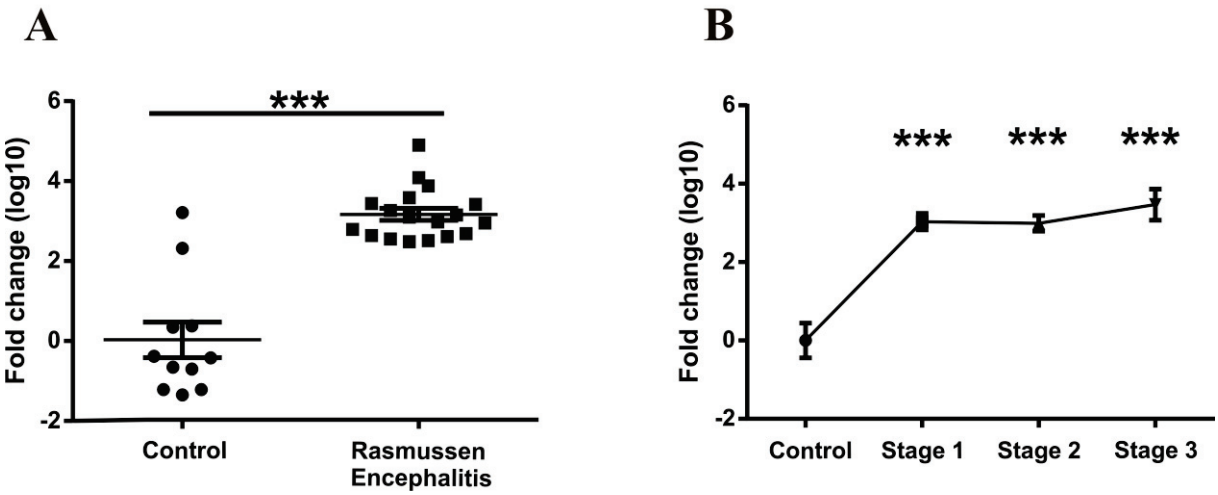

Figure 10. IL-1β quantification by real time qPCR. *(A) IL-1β quantification in cortex area in patients from control group (n=11) and the pool of RE cases (n=18). The RE group is compared to the control group. (B) Representation of IL-1β positive cells in the control group (n=11), stage 1 of RE (n=7), stage 2 (n=6) and stage 3 (n=5). Each RE stage is compared to the control group. (***p<0,001). Data is shown as mean ± SEM.*

The same statistical analyses and representation was done for IL-1R1 mRNA quantification (Figure 11). Once more the pool of RE stages was compared to the control group. RE group presented a value significantly higher than the value from control group (Figure 11A). Comparing each stage of RE with the control group (Figure 11B), revealed significant upregulation of IL-1R1 in each stage. From stage 1 to 3 the line of the graph was rising (Figure 11B) but statistical analysis concluded that there were no significant differences between stages.

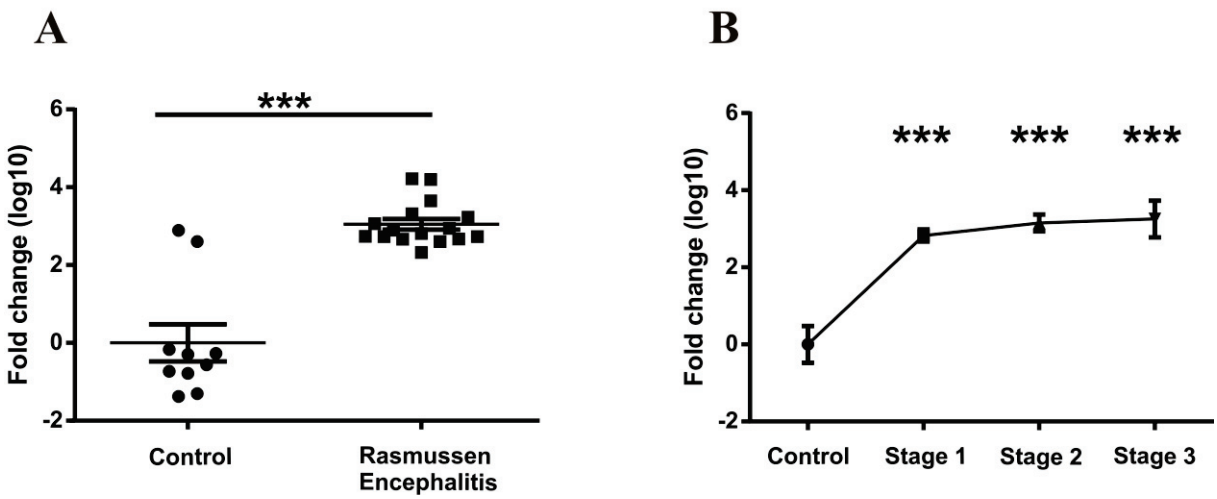

Figure 11. IL-1R1 quantification by real time qPCR. *(A) IL-1R1 quantification in cortex area in patients from the control group (n=10) and the pool of RE cases (n=18). (B) Representation of IL-1R1 positive cells in the control group (n=10), stage 1 of RE (n=6), stage 2 (n=7) and stage 3 (n=3). Each RE stage is compared to the control group. (***p<0,001). Data is shown as mean ± SEM.*

6.3 Analysis of IL-1β in RE by qualitative and quantitative immunohistochemistry

One of the main goals of the project was to confirm the presence of IL-1β in RE as well as to quantify the protein in different stages of the disease. Western blot technique did not allow the detection and quantifying the cytokine. Nonetheless, IHC staining and cell counting were performed so as to achieve the goals.

All the study cases (control and RE samples) were stained for IL-1β following the standard light microscopy staining procedure. The stainings were compared with stainings for IL-1β in other diseases (Figure 12). As expected, the negative control did not present positive cells (Figure 12A). Herpes simplex virus (HSV) (Figure 12B) and Rhesus monkey with EAE (Figure 12C) however revealed a very high number of widely spread IL-1β positive cells. In the case of Rhesus monkey, positive cells were also observed in nodules or around blood vessels (Figure 12C). In the RE samples, IL-1β positive cells were present in microglia nodules (Figure 12D-F) as well as around blood vessels. The distribution pattern of the cells is similar to the one in Rhesus monkey. It is important to mention that the number of IL-1β cells in RE was notable lower than in the sample of HSV or Rhesus monkey.

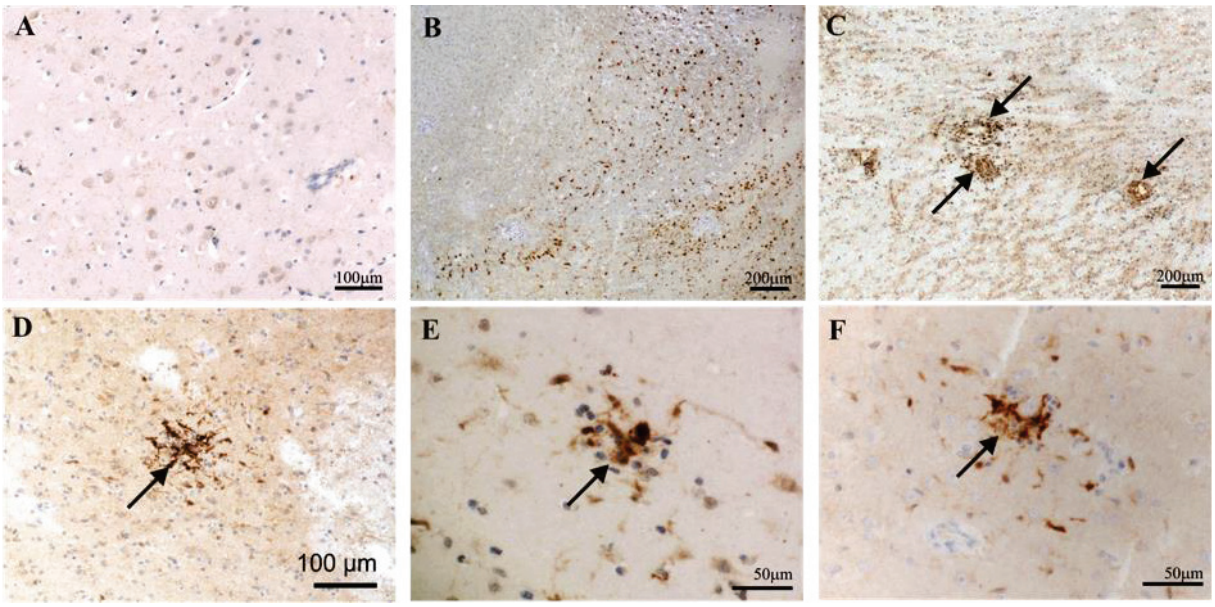

Figure 12. Immunohistochemistry staining for IL-1β in different diseases. *(A) Negative control with no IL-1β positive cells. (B) HSV sample with IL-1β positive cells occupying a large area. (C) Rhesus monkey with EAE with IL-1β positive cells around blood vessels. (D-F) RE cases with IL-1β microglia nodules are marked with arrows.*

Additionally, the distribution and quantity of IL-1β positive cells compared to Caspase-1 positive cells was investigated in Rhesus monkey. A staining for IL-1β and another for Caspase-1 on consecutive sections (Y318/10/2) showed that Caspase-1 positive cells (Figure 13B) were more abundant than the IL-1β (Figure 13A). IL-1β positive cells and Caspase-1 positive cells were mainly found around blood vessels. IL-1β positive cells were observed in microglia nodules and Caspase-1 positive cells were widely spread on the sample. Furthermore, IL-1β positive cells seemed to be a subpopulation of the Caspase-1 positive cells. This expression pattern was elucidated with the confocal microscopy.

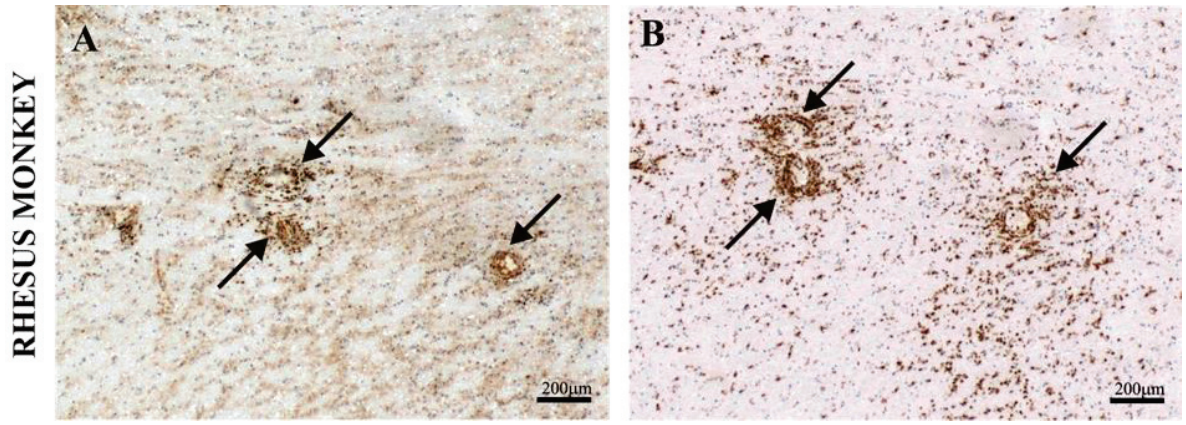

Figure 13. Immunohistochemistry staining for IL-1β and Caspase-1 in Rhesus monkey*. (A) IL-1β positive cells. Microglia nodules and positive cells around blood vessels are pointed out with arrows.*

(B) Caspase-1 positive cells are concentrated around blood vessels and they are also found in the rest of the tissue.

With the help of a morphometric grid and the light microscope, the IL-1β positive cells were counted in the same areas that were used for the real time qPCR experiments. After counting, all the RE stages were pooled into one group that was compared with the control group. The Mann-Whitney U-test revealed that the values obtained from the RE group were significantly higher than the ones from control (Figure 14A). Furthermore, the RE stages were analyzed individually and each of them was compared to the control group. In this case, Kruskal-Wallis test with post-hoc Dunn's multiple comparisons test confirmed that every stage presented significantly higher values compared to the control (Figure 14B), however, no significant difference was found between stages.

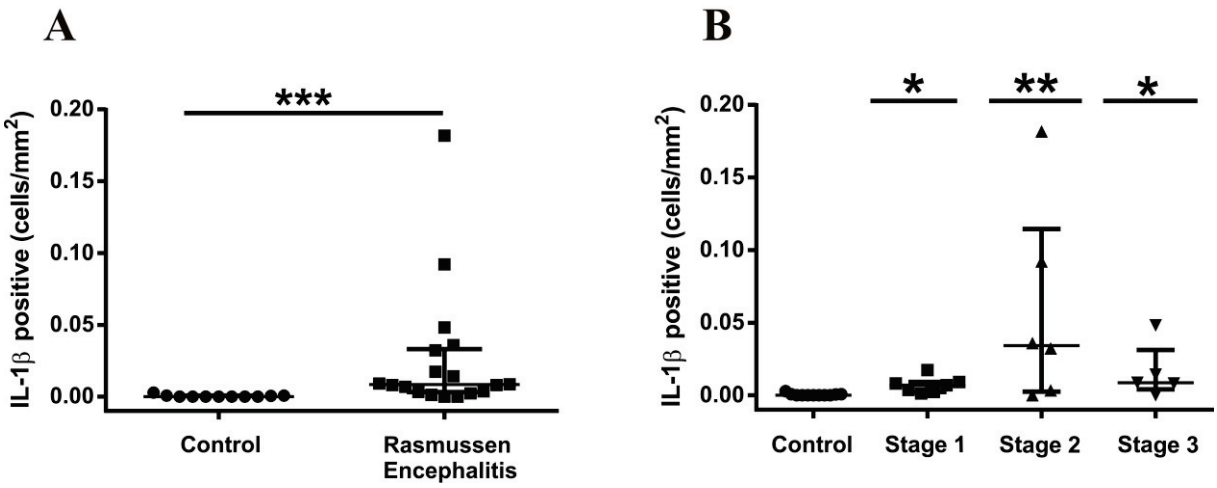

Figure 14. Quantification of the number of IL-1β positive cells in Rasmussen encephalitis. *(A) Quantification of IL-1β positive cells per mm^2 in patients from the control group (n=11) and the pool of RE cases (n=18). The RE group is compared to the control group. (B) Representation of IL-1β positive cells in the control group (n=11), stage 1 of RE (n=7), stage 2 (n=6) and stage 3 (n=5). Each RE stage is compared to the control group. (*p<0,05; **p<0,01; ***p<0,001) Data is shown as median ± interquartile range (IQR).*

6.4 Analysis of Cell-type specific expression of IL-1β and Caspase-1 by confocal laser fluorescence microscopy in Rhesus monkey with EAE and Rasmussen Encephalitis

In the project the type of cells that express IL-1β and/or Caspase-1 were elucidated in RE disease as well as in Rhesus monkey with EAE. In order to achieve this goal, FFPE tissue from human and monkey was stained for the cytokine and the enzyme in combination with markers for microglia and astrocytes. Fluorescence double and triple stainings were performed and analyzed by confocal laser microscopy.

By doing a triple staining for Caspase-1, IL-1β and a marker for astrocytes (GFAP) in the monkey and the human sample (Figure 15), it was shown that both, cytokine and enzyme, were expressed in the same cells, however these cells were not astrocytes. Furthermore, it was confirmed that the number of positive cells for Caspase-1 was higher than the number of IL-1β positive cells and therefore, not all the Caspase-1 positive cells were also IL-1β positive.

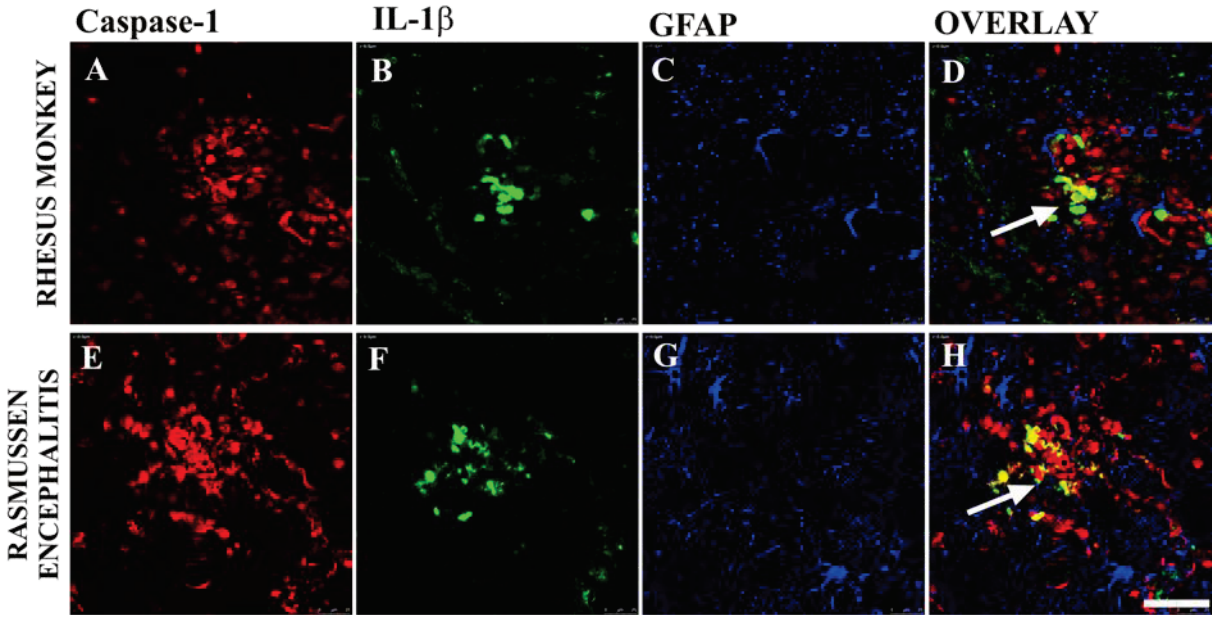

Figure 15. Confocal laser fluorescence microscopy of Caspase-1 and IL-1β in Rhesus monkey and RE. *(A, E) Caspase-1 is shown in red (Cy3) (B, F) IL-1β is labeled in green (Cy2). (C, G) GFAP is labeled in blue (Dylight649). (D, H) Overlay of the fluorophores. Colocalization is observed for Caspase-1 and IL-1β. (Panels A-H used a scale bar of 50μm).*

After confirming by confocal laser microscopy that cytokine and enzyme were expressed in the same cells, the next question to address was which type of cells expresses them. A double staining for IL-1β and a marker for microglia (Iba-1) was done again in human RE and

Rhesus monkey and it revealed that the cytokine is expressed in microglia although not all the cells were expressing IL-1β (Figure 16).

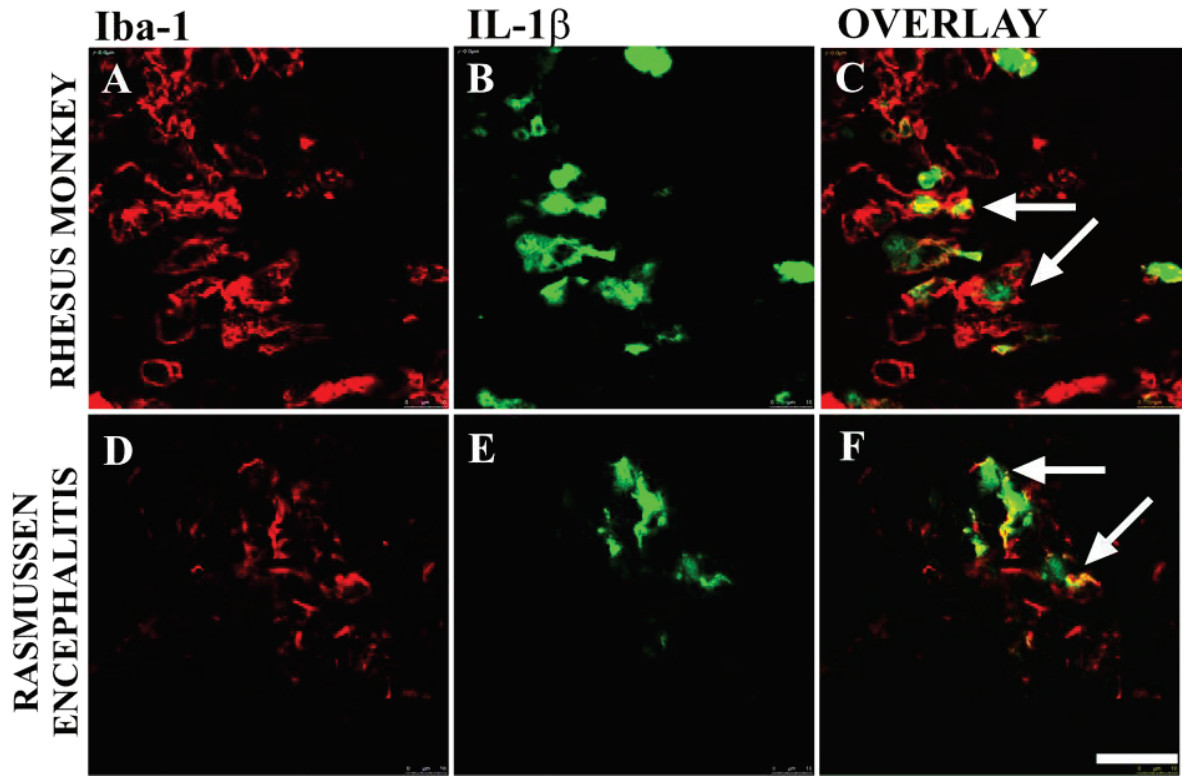

Figure 16. Confocal laser fluorescence microscopy of IL-1beta in Rhesus monkey and RE. *(A, D) Iba-1 is labeled in red (Cy3). (B, E) IL-1β is shown in green (Cy2). (C, F) Overlay of both fluorophores showing colocalization of Iba-1 and IL-1β. (Panels A-F used a scale bar of 20μm).*

A similar staining was done with Caspase-1. In the case of Rhesus monkey, a triple staining was performed with Caspase-1, Iba-1 and GFAP (Figure 17). Once again, it was found that Caspase-1 was not expressed in astrocytes but in this case it was visible that it was produced by microglia (Figure 17).

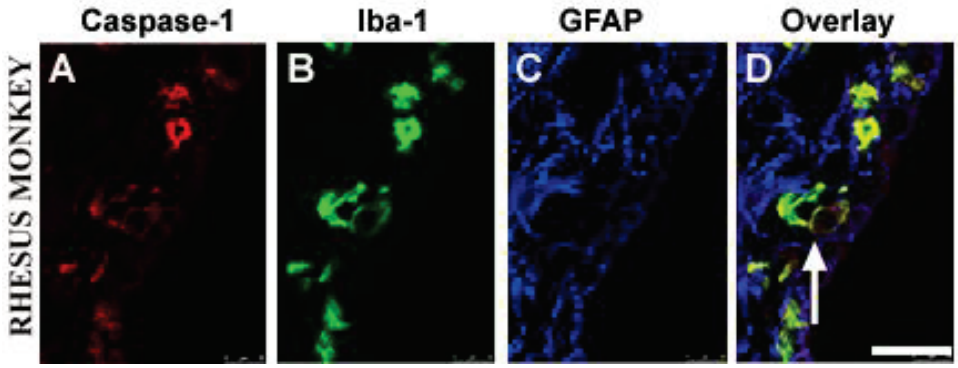

Figure 17. Confocal fluorescence microscopy of Caspase-1 in Rhesus monkey. *(A) Caspase-1 is labeled in red (Cy3). (B) Iba-1 is shown in green (Cy2). (C) GFAP is labeled in blue (Dylight649). (D) Overlay of fluorophores. Capase-1 is overlapped with Iba-1 but not with GFAP. (Panels A-D used a scale bar of 20μm).*

A double staining was done for Caspase-1 and Iba-1 with the RE sample (Figure 18). As well as in the monkey, it was shown that Caspase-1 is presented in microglia (Figure 18).

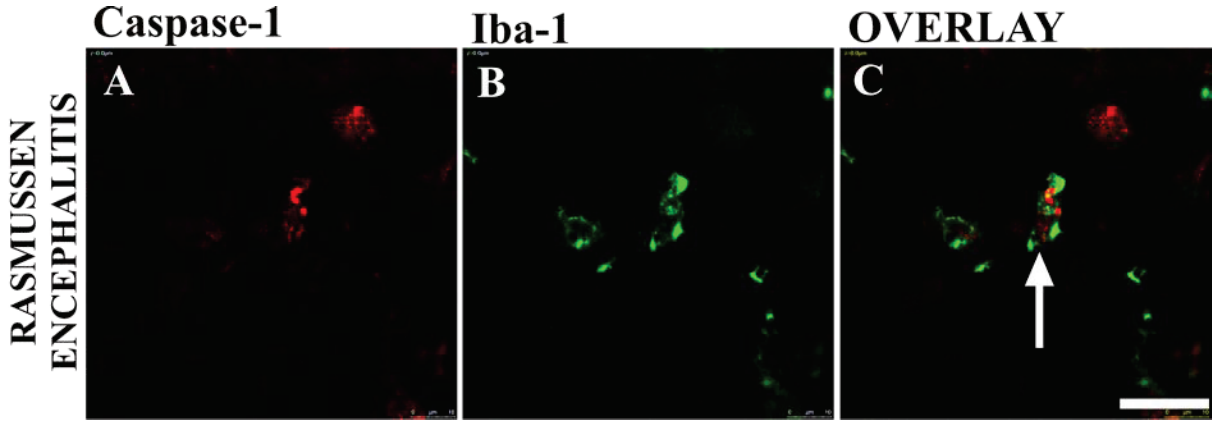

Figure 18. Confocal fluorescence microscopy of Caspase-1 in RE. *(A) Caspase-1 is labeled in red (Cy3). (B) Iba-1 is shown in green (Cy2). (C) Overlay of fluorophores. Capase-1 is overlapped with Iba-1. (Panels A-C used a scale bar of 20μm).*

6.5 Cell-type determination of expression of IL-1R1 by confocal laser fluorescence microscopy in Rasmussen Encephalitis

As part of the project the type of cells that express IL-1R1 in RE disease was also elucidated. In order to achieve this goal, cryopreserved tissue from human was stained for the receptor

but also with markers for microglia, astrocytes and neurons. Fluorescence double and triple stainings were performed and analyzed by confocal laser microscopy.

Firstly, a triple staining for IL-1R1, GFAP and nuclei staining (DAPI) was done. It was observed that the receptor for IL-1β was expressed in astrocytes (Figure 19). The arrows on the picture mark two astrocytes overlapping with the receptor signal (Figure 19D).

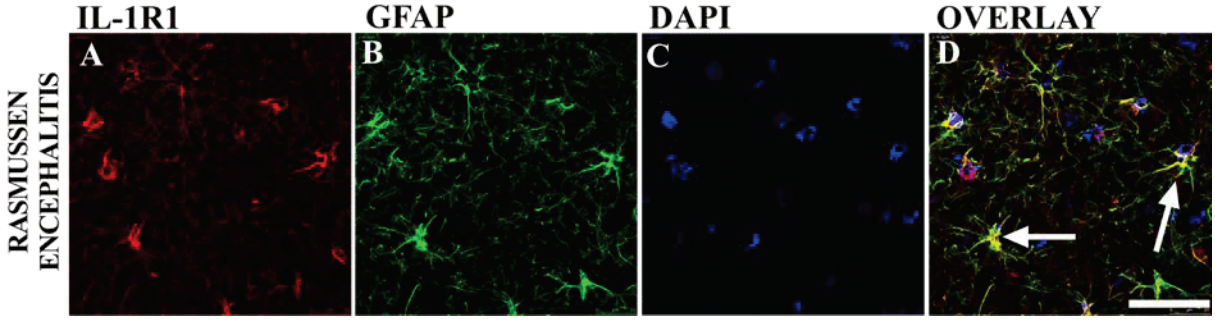

Figure 19. Confocal laser fluorescence microscopy of IL-1R1 in RE. *(A) IL-1R1 is labeled in red (Cy3). (B) GFAP is shown in green (Cy5). (C) The nuclei of the cells is shown in blue (DAPI). (D) Overlay of fluorophores. IL-1R1 is colocalized with GFAP. (Panel A-D used a scale bar of 50μm).*

It was also tested if the receptor was present in microglia. For this purpose, a triple staining was performed for IL-1R1, GFAP and a microglia marker (CD68) and it was found that the receptor was expressed in microglia as well as in astrocytes (Figure 20). The arrow on the right marked an astrocyte with IL-1R1 and the arrow on the left indicated a microglia also with the receptor (Figure 20D).

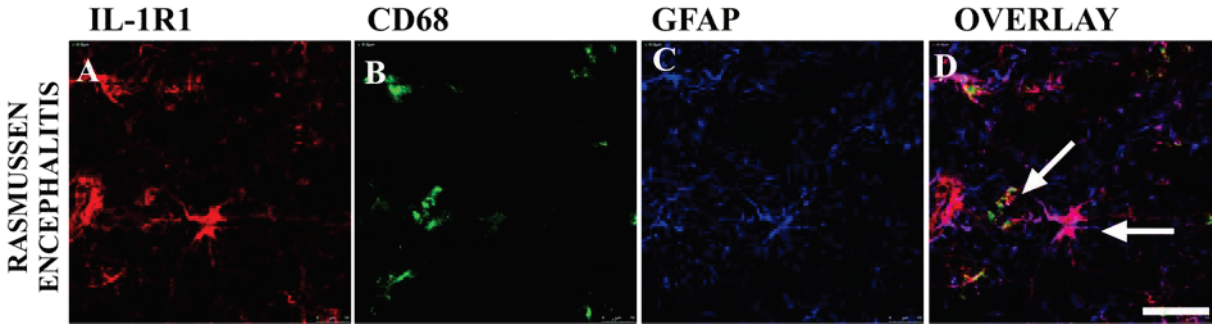

Figure 20. Confocal laser fluorescence microscopy of IL-1R1 in RE. *(A) IL-1R1 is labeled in red (Cy3). (B) CD68 is shown in green (Cy2). (C) GFAP is labeled in blue (Cy5). (D) Overlay of fluorophores. IL-1R1 is colocalized with GFAP and also with CD68. (Panel A-D used a scale bar of 20μm).*

Another staining was done in order to see if IL-1R1 was expressed also in neurons. Therefore a double staining for the receptor and a marker of neurons (Neu-N) was performed (Figure 21). The arrows pointed to two neurons that express the IL-1 receptor (Figure 21C).

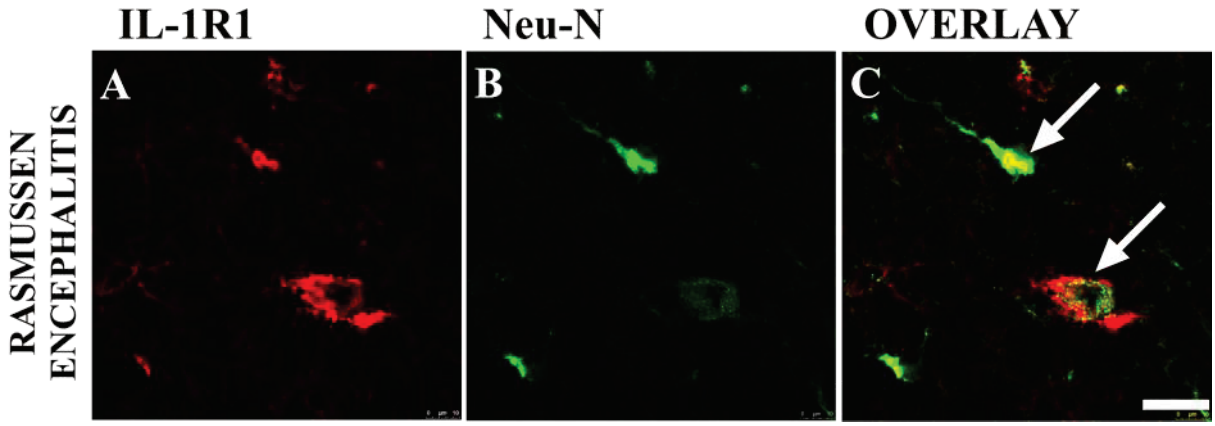

Figure 21. Confocal laser fluorescence microscopy of IL-1R1 in RE. *(A) IL-1R1 is labeled in red (Cy3). (B) NeuN is shown in green (Cy2). (C) Overlay of fluorophores. IL-1R1 and Neu-N are colocalized. (Panel A-C used a scale bar of 20μm).*

7 Discussion

Several studies have elucidated the role of inflammation in many diseases in the CNS. Among all the pro-inflammatory molecules, the cytokine IL-1β is one of the best-studied mediators which has been proposed as a key player in the regulation of the inflammatory response in many neurological diseases (Sankowski et al., 2015). In particular, animal models of epilepsy have provided confirmation that experimentally provoked seizures trigger an inflammatory response in the CNS and a large range of inflammatory substances are produced during this response (Bauer and Bien, 2009). In human epilepsy, the implication of inflammatory mediators from the innate immune system in pathological damage to the brain and induction of seizures are largely unknown (Bauer and Bien, 2009). However, it has been shown that IL-1β is involved both in inflammation and epilepsy. Thus, it could be speculated that this cytokine assume similar roles in RE as in epilepsy, as epileptic seizures and chronic brain inflammation are characteristics of this condition. In fact, there is a recent support for a pathogenic role of IL-1β, release, from microglia, in RE. Ramaswamy et al. revealed in RE patients the involvement of cortex and white matter in the disease process with a simultaneous induction of inflammasome components. They showed that the inflammasome activation is highest in microglia and its induction triggers selective release of IL-1β by microglia, but not astrocytes (Ramaswamy et al., 2013). Nevertheless Ramaswamy et al. only showed this data in 4 cases and did not investigate different stages of the disease.

This thesis was focused on RE disease and aimed to give further insights into the possible role and the cell-type expression of IL-1β, its receptor IL-1R1 and Caspase-1, the enzyme that cleaves the inactive pro-IL-1β producing the mature and biologically active form of IL-1β (17kDa).

In the case of diseases where the CNS is affected, FFPE tissue repositories provide a wealth of information for researchers. Nevertheless, working with FFPE tissue present several challenges that may be encountered upon performing the experiments and analyzing the final data. Formaldehyde is a cross-linking reagent that leads to the generation of protein-nucleic acid and covalent protein-protein cross-links, and causes nucleic acids to fragment or modify because of fixation process conditions (Lin et al., 2009; Scicchitano et al., 2009). This makes it very difficult to perform protein, DNA and RNA extraction and amplify high molecular weight DNA. Cross-linking also blocks polymerase chain reaction (PCR) amplification (Lin et al., 2009) and compromise the use of RNA as a substrate for reverse transcription. Moreover, the fixation process covalently modifies RNA by the addition of monomethyl groups to the bases making the molecules rigid and susceptible to mechanical shearing (Masuda et al., 1999).

The access to the “locked proteome” in FFPE tissue has been recently achieved with the development and application of various protein extraction strategies and successful results have been obtained (Addis et al., 2009). Addis et al. 2009 described a protein extraction

method from FFPE tissue, which is versatile, reliable and amenable to several downstream methodologies and applicable to different analytical platforms. Based on this protocol, the quantification of IL-1β from FFPE tissue was performed followed by western blot as analytical platform. However, only a band around 42kDa corresponding to β-actin was detected, but none of the samples presented a band for IL-1β around 17kDa. The results of β-actin confirmed that the protein extraction protocol as well as the rest of the process including the quantification method (Western blot) worked and it was correctly executed. The reason(s) why the cytokine was not detected could be due to the problems derived from the cross-links with nucleic acids. The protein could be lost along the extraction process and the detergent, such as SDS, in the extraction buffer could also interfere with detection. It could also happen that the blotting time was too long and the cytokine crossed also the membrane because of its small size. Nevertheless, the most probable explanation is that the initial concentration of the protein in the samples is already under detection level.

Facing the impossibility of quantifying IL-1β by western blot, the project was focused on comparing the expression of IL-1β and IL-1R1 at mRNA level in the cortical grey matter of RE patients and control samples. This study detected significantly up-regulated IL-1β and IL-1R1 mRNA within RE samples compared to controls. RE patients present neuroinflammation and it was expected these samples to have higher values of the pro-inflammatory cytokine compared to the control samples. The data obtained for IL-1R1 was consistent with the expectations. IL-1R1 is also involved in the inflammation response, thus we found up-regulated values in the RE samples. Moreover, the expression of IL-1β and IL-1R1 mRNA of each stage was compared to control group. All of them had significantly higher levels either of IL-1β or IL-1R1 compared to control group. As the progression of the disease takes place, the stages vary from early inflammation defined by infiltration of T lymphocytes and neuroglial reactions, to more severe stages with extensive neuronal cell death and cavitation of the cerebral cortex (Pardo et al., 2004), therefore it could be expected that the values of IL-1β and IL-1R1 between stages were different but this is not shown in our results. There are no significant differences, in terms of IL-1β and IL-1R1 expression between different stages. Our data confirm the results from Ramaswamy et al. where IL-1β transcript levels were increased in the white matter of RE patients compared to non-RE samples, as well as it happened in cortex (Ramaswamy et al., 2013). A possible explanation why no differences between the different stages were found could be the classification of the samples in 3 different stages. The categorization of the samples cannot be always entirely strict, meaning, there is a gradual change between the different stages and some of the samples could be classified between two different stages. Other interpretation of these results could be that at stage 1 the maximum receptor density has been reached and the little neuronal cell loss does not change the total values. The same could be applied for IL-1β values, reaching the highest expression level at stage 1 and the little changes in microglia activation does not change the total values.

For detection and quantification of cytokine IL-1β, IHC staining was performed in the RE and control cases. Firstly, we demonstrated the presence of IL-1β protein in RE. The distribution

of IL-1β positive cells was compared with other diseases also stained for IL-1β. RE samples presented a very heterogeneous distribution of IL-1β positive cells but the presence of IL-1β in microglia nodules and around blood vessels were two common denominators in many of the cases. Furthermore, it was shown that the number of IL-1β positive cells is clearly lower than the cells expressing Caspase-1. Caspase-1 is already expressed as part of the inflammasome and it is also involved in activation of IL-18. However, IL-1β does not have to be necessarily expressed in all the Caspase-1 positive cells but in the cells that have received both activation signals and therefore synthesized first and then processed the protein (Kwak et al., 2016). Cytokine and enzyme were expressed in microglia nodules as well as around blood vessels, additionally Caspase-1 was also expressed in individual cells throughout the sample. Moreover, IL-1β positive cells from RE cases and control group were counted under the light microscope and the results confirmed the data obtained by qPCR; namely, the number of IL-1β positive cells in RE stainings were significantly higher than control group. As well, each RE stage compared to controls presented significantly increased values. However, no difference was observed between the stages.

To conclude, it was very important to elucidate the cell-type expression of IL-1β, its receptor and Caspase-1. The major source of IL-1β in pathologic tissue is represented by activated glial cells but this cytokine has also been found expressed by neurons both in experimental models and in human epileptic tissue (Thompson and Tsirka, 2017; Vezzani, 2015). In the case of RE and Rhesus monkey with EAE, we have shown that the situation is not exactly as explained above. We found Caspase-1 and IL-1β expression in microglia but not in astrocytes. One reason why our results differed from other studies might be that there is a difference between the IL-1β expression in rodents and humans and between RE and other epileptic diseases. Other explanation might be the different interpretation of the results. Like in other epileptic diseases, our IHC stainings showed a weak signal for IL-1β in astrocytes and neurons. However, because we did not find a Caspase-1 signal in these cells in the confocal stainings, we interpreted the astrocytic and neuronal staining as background rather than specific staining for IL-1β. The confocal stainings confirmed the immunohistochemistry being Caspase-1 positive cells more abundant than IL-1β. In the case of IL-1R1, we confirmed that microglia, astrocytes and also neurons express the receptor.

These results suggest that since microglia produce IL-1β and also express IL-1R1, it appears that this cytokine is endowed with autocrine and paracrine actions, exerting effects on astrocytes and neurons that also express the receptor and triggering other pro-inflammatory pathways and possibly affecting the neuronal excitability (Vezzani and Baram, 2007). Moreover, the study indicated a correlation between enhanced IL-1β expression and RE pathology even though the potential functional role that IL-1β may play in RE remains to be directly demonstrated. In addition, this project provides further insight into the complex role of inflammation in the generation and exacerbation of epilepsy, specifically in Rasmussen encephalitis, and contributes to the development of new molecular targets for the design of

antiepileptic drugs, which might not only inhibit the epileptic seizures, but, since IL-1β is a pro-inflammatory cytokine, might also influence the immunological response.

Several questions remain opened for further investigations, such as which pathways are triggered by IL-1β, which, in turn, lead to chronic inflammation in RE. Another interesting question is the presence of IL-1β and caspase-1 in epilepsies without adaptive immunity involvement, like infiltration of T-cells. Last but not least, further characterization of the inflammasome in RE is required and the presence of IL-18 has yet to be elucidated.

8 Abbreviations

Ab	Antibody
a.d.	Deionized water
AIM2	Absent in melanoma 2
ASC	Apoptosis-associated speck-like protein containing a CARD
AP1	Activator protein 1
APS	Ammonium persulfate
Asp	Aspartic acid
ATP	Adenosine triphosphate
BBB	Blood-brain barrier
cDNA	Complementary DNA
C	Control
CARD	Caspase activation and recruitment domain
CD	Cluster of differentiation
CNS	Central nervous system
COX	Cyclooxygenase
CSA	Catalysed signal amplification system
CTX	Cortex
Cy	Cyanine dye
ddH_2O	double-distilled water
DAB	3, 3'-Diaminobenzidine
DAMP	Damage-associated molecular pattern
DAPI	4', 6'-diamidino-2-phenylindole
DNA	Deoxyribonucleic acid
EAE	Experimental Autoimmune Encephalomyelitis
EDTA	Ethylenediaminetetraacetic acid
EtOH	Ethanol
fg	Femtogram

FCS	Fetal calf serum
FFPE	Formalin-fixed, paraffin-embedded
FIIND	Function to find domain
g	Gram
g	G-force
G	Gauge
GABA	γ-aminobutyric acid
GAPDH	Glycerinaldehyd-3-phosphate dehydrogenase
GFAP	Glial fibrillary acidic protein
GluR3	Glutamate receptor 3
H_2O_2	Hydrogen peroxide
HCl	Hydrochloric acid
HE	Hemalaun-Eosin
HMGB1	High-mobility group box
HRP	Horseradish Peroxidase
HSV	Herpes simplex virus
Iba-1	Ionized calcium binding adaptor molecule 1
IHC	Immunohistochemistry
IL-18	Interleukin 18
IL-1β	Interleukin 1 beta
IL-1R1	Interleukin 1 receptor 1
IS	Immune system
$KHCO_3$	Potassium bicarbonate
l	Left
L	Liter
LRR	Leucine rich repeat
M	Molarity
MAPK	Mitogen-activated protein kinase

MDP	Muramyl dipeptide
$MgSO_4$	Magnesium sulfate
MHC	Major histocompatibility complex
min	Minutes
ml	Milliliter
mm	Milimeter
mM	Milimolar
mRNA	Messenger ribonucleic acid
μm	Micrometer
μl	Microliter
ng	Nanogram
nM	Nanomolar
N	Normality
NACHT	NAIP, CIITA, HET-E and TP-1- domain
NaCl	Sodium chloride
NaH_2PO_4	Monosodium phosphate
Neu-N	neuronal nuclear antigen
NKκB	Nuclear factor kappa B
NK	Natural killer
NMDA-R	N-methyl-D-aspartate-receptor
NOD	NOD-like receptor
pg	picogram
PAMP	Pathogen-associated molecular pattern
PBS	Phosphate buffer solution
PCR	Polymerase chain reaction
PI3K	Phosphatidylinositol-4,5-bisphosphate 3-kinase
PLA2	Phospholipase A2
PRR	Pattern-recognition receptor

PVDF	Polyvinylidene difluoride
PYD	Pyrin domain
qPCR	Quantitative polymerase chain reaction
r	Right
rcf	Relative centrifugal force
rpm	Revolution per minute
rRNA	ribosomal ribonucleic acid
RE	Rasmussen encephalitis
RT	Room temperature
SDS	Sodium dodecyl sulphate
SEM	Standard error of the mean
TBS	Tris-buffered saline
TBST	Tris-buffered saline with Tween 20
tc	Temporal cortex
TEMED	Tetramethylenediamine
TGF-β	Transforming growth factor β
TLR	Toll-like receptor
TNF-α	Tumor necrosis factor alpha
V	Volt

9 References

Addis, M.F., Tanca, A., Pagnozzi, D., Crobu, S., Fanciulli, G., Cossu-Rocca, P., Uzzau, S., 2009. Generation of high-quality protein extracts from formalin-fixed, paraffin-embedded tissues. Proteomics 9, 3815–3823.

Antonelli, M., Kushner, I., 2017. It's time to redefine inflammation. FASEB J. fj.201601326R.

Bauer, J., Bien, C.G., 2009. Encephalitis and epilepsy. Semin. Immunopathol. 31, 537–544.

Becker, K., 2006. Innate and adaptive immune responses in CNS disease. Clin. Neurosci. Res. 6, 227–236.

Berger, T., Rubner, P., Schautzer, F., Egg, R., Ulmer, H., Mayringer, I., Dilitz, E., Deisenhammer, F., Reindl, M., 2003. Antimyelin antibodies as a predictor of clinically definite multiple sclerosis after a first demyelinating event. N. Engl. J. Med. 349, 139–45.

Bien, C.G., Bauer, J., Deckwerth, T.L., Wiendl, H., Deckert, M., Wiestler, O.D., Schramm, J., Elger, C.E., Lassmann, H., 2002. Destruction of neurons by cytotoxic T cells: A new pathogenic mechanism in Rasmussen's encephalitis. Ann. Neurol. 51, 311–318.

Bryant, C., Fitzgerald, K.A., 2009. Molecular mechanisms involved in inflammasome activation. Trends Cell Biol. 19, 455–464.

Chen, G., Shaw, M.H., Kim, Y.-G., Nez, G.N., 2009. NOD-Like Receptors: Role in Innate Immunity and Inflammatory Disease Key Words. Annu. Rev. Pathol. Mech. Dis 4, 365–98.

De Rivero Vaccari, J.P., Dietrich, W.D., Keane, R.W., 2016. Therapeutics targeting the inflammasome after central nervous system injury. Inj. Transl. Res. J. Lab. Clin. Med. 167, 35–45.

Devinsky, O., Vezzani, A., Najjar, S., De Lanerolle, N.C., Rogawski, M.A., 2017. Glia and epilepsy: excitability and inflammation. Trends Neurosci. 36, 174–184.

Edye, M.E., Walker, L.E., Sills, G.J., Allan, S.M., Brough, D., 2014. Epilepsy and the

inflammasome: Targeting inflammation as a novel therapeutic strategy for seizure disorders. Inflammasome 1, 36–43.

Freeman, L.C., Ting, J.P.Y., 2016. The pathogenic role of the inflammasome in neurodegenerative diseases. J. Neurochem. 136, 29–38.

Guo, H., Callaway, J.B., Ting, J.P.-Y., 2015. Inflammasomes: mechanism of action, role in disease, and therapeutics. Nat. Med. 21, 677–687.

Gustin, A., Kirchmeyer, M., Koncina, E., Felten, P., Losciuto, S., Heurtaux, T., Tardivel, A., Heuschling, P., Dostert, C., 2015. NLRP3 inflammasome is expressed and functional in mouse brain microglia but not in astrocytes. PLoS One 10, 1–19.

Jha, M.K., Lee, H.-W., Kim, S., Suk, K., 2015. Innate immune proteins as biomarkers for CNS injury: critical evaluation (WO 2013119673 A1). Expert Opin. Ther. Pat. 25, 241–245.

Khansari, N., Shakiba, Y., Mahmoudi, M., 2009. Chronic inflammation and oxidative stress as a major cause of age-related diseases and cancer. Recent Pat. Inflamm. Allergy Drug Discov. 3, 73–80.

Kwak, A., Lee, Y., Kim, H., Kim, S., 2016. Intracellular interleukin (IL)-1 family cytokine processing enzyme. Arch. Pharm. Res. 39, 1556–1564.

Lin, J., Kennedy, S.H., Svarovsky, T., Rogers, J., Kemnitz, J.W., Xu, A., Zondervan, K.T., 2009. High-quality genomic DNA extraction from formalin-fixed and paraffin-embedded samples deparaffinized using mineral oil. Anal. Biochem. 395, 265–267.

Marchi, N., Granata, T., Janigro, D., 2014. Inflammatory pathways of seizure disorders. Trends Neurosci 37, 55–65.

Martinon, F., Burns, K., Tschopp, J., 2002. The Inflammasome: A molecular platform triggering activation of inflammatory Caspases and processing of proIL-β. Mol. Cell 10, 417–426.

Masuda, N., Ohnishi, T., Kawamoto, S., Monden, M., Okubo, K., 1999. Analysis of chemical modification of RNA from formalin-fixed samples and optimization of molecular

biology applications for such samples. Nucleic Acids Res. 27, 4436–4443.

Matin, N., Tabatabaie, O., Falsaperla, R., Lubrano, R., Pavone, P., Mahmood, F., Gullotta, M., Serra, A., Di Mauro, P., Cocuzza, S., Vitaliti, G., 2015. Epilepsy and innate immune system: A possible immunogenic predisposition and related therapeutic implications. Hum. Vaccines Immunother. 11, 2021–2029.

Meng, X.-F., Tan, L., Tan, M.-S., Jiang, T., Tan, C.-C., Li, M.-M., Wang, H.-F., Yu, J.-T., 2014. Inhibition of the NLRP3 inflammasome provides neuroprotection in rats following amygdala kindling-induced status epilepticus. J. Neuroinflammation 11, 212.

Netea, M.G., Simon, A., Van De Veerdonk, F., Kullberg, B.J., Van Der Meer, J.W.M., Joosten, L.A.B., 2010. IL-1β processing in host defense: Beyond the inflammasomes. PLoS Pathog. 6.

Orozco LD, Bennett BJ, Farber CRChe, N., Wen, P., Qi, H.X., Mutukulu, A., Siemers, N., 2012. Unraveling inflammatory responses using systems genetics and gene-environment interactions in macrophages. Cell. 2012 151, 658–670.

Pardo, C.A., Vining, E.P.G., Guo, L., Skolasky, R.L., Carson, B.S., Freeman, J.M., 2004. The Pathology of Rasmussen Syndrome: Stages of Cortical Involvement and Neuropathological Studies in 45 Hemispherectomies. Epilepsia 45, 516–526.

Ramaswamy, V., Walsh, J.G., Sinclair, D.B., Johnson, E., Tang-Wai, R., Wheatley, B.M., Branton, W., Maingat, F., Snyder, T., Gross, D.W., Power, C., 2013. Inflammasome induction in Rasmussen's encephalitis: cortical and associated white matter pathogenesis. J. Neuroinflammation 10, 152.

Rasmussen, T., Olszewski, J., Lloyd-Smith, D., 1958. Focal seizures due to chronic localized encephalitis. Neurology 8, 435–445.

Ravizza, T., Boer, K., Redeker, S., Spliet, W.G.M., van Rijen, P.C., Troost, D., Vezzani, A., Aronica, E., 2006. The IL-1β system in epilepsy-associated malformations of cortical development. Neurobiol. Dis. 24, 128–143.

Ravizza, T., Gagliardi, B., Noé, F., Boer, K., Aronica, E., Vezzani, A., 2008. Innate and adaptive immunity during epileptogenesis and spontaneous seizures: Evidence from

experimental models and human temporal lobe epilepsy. Neurobiol. Dis. 29, 142–160.

Ravizza, T., Lucas, S.M., Balosso, S., Bernardino, L., Ku, G., Noé, F., Malva, J., Randle, J.C.R., Allan, S., Vezzani, A., 2006. Inactivation of Caspase-1 in rodent brain: A novel anticonvulsive strategy. Epilepsia 47, 1160–1168.

Rogers, S.W., Andrews, P.I., Gahring, L.C., Whisenand, T., Cauley, K., Crain, B., Hughes, T.E., Heinemann, S.F., Mcnamara, J.O., Rogers, S.W., Andrews, P.I., Gahring, L.C., Whisenand, T., Cauley, K., Crain, B., Hughes, T.E., Heinemann, S.F., Mcnamara, J., 1994. Autoantibodies to Glutamate Receptor GIuR3 in Rasmussen ' s Encephalitis. Science (80-.). 265, 648–651.

Sankowski, R., Mader, S., Valdés-Ferrer, S.I., 2015. Systemic inflammation and the brain: novel roles of genetic, molecular, and environmental cues as drivers of neurodegeneration. Front. Cell. Neurosci. 9, 28.

Schneider-Hohendorf, T., Mohan, H., Bien, C.G., Breuer, J., Becker, A., Görlich, D., Kuhlmann, T., Widman, G., Herich, S., Elpers, C., Melzer, N., Dornmair, K., Kurlemann, G., Wiendl, H., Schwab, N., 2016. CD8(+) T-cell pathogenicity in Rasmussen encephalitis elucidated by large-scale T-cell receptor sequencing. Nat. Commun. 7, 11153.

Schroder, K., Tschopp, J., 2010. The Inflammasomes. Cell 140, 821–832.

Scicchitano, M.S., Dalmas, D.A., Boyce, R.W., Thomas, H.C., Frazier, K.S., Journal, T., 2009. Enables Robust Proteomic Profiles by Mass Spectrometry. J. Histochem. Cytochem. 57, 849–860.

Scott, G., Mahmud, M., Owen, D.R., Johnson, M.R., 2016. Microglial positron emission tomography (PET) imaging in epilepsy: Applications, opportunities and pitfalls. Seizure 44, 42–47.

Takahashi, Y., Mori, H., Mishina, M., Watanabe, M., Fujiwara, T., Shimomura, J., Aiba, H., Miyajima, T., Saito, Y., Nezu, A., Nishida, H., Imai, K., Sakaguchi, N., Kondo, N., 2003. Autoantibodies to NMDA receptor in patients with chronic forms of epilepsia partialis continua. Neurology 61, 891–6.

Takei, H., Wilfong, A., Malphrus, A., Yoshor, D., Hunter, J. V., Armstrong, D.L., Bhattacharjee, M.B., 2010. Dual pathology in Rasmussen's encephalitis: A study of seven cases and review of the literature. Neuropathology 30, 381–391.

Thompson, K., Tsirka, S., 2017. The Diverse Roles of Microglia in the Neurodegenerative Aspects of Central Nervous System (CNS) Autoimmunity. Int. J. Mol. Sci. 18, 504.

van de Veerdonk, F.L., Netea, M.G., Dinarello, C.A., Joosten, L.A.B., 2011. Inflammasome activation and IL-1β and IL-18 processing during infection. Trends Immunol. 32, 110–116.

Varadkar, S., Bien, C.G., Kruse, C.A., Jensen, F.E., Bauer, J., Pardo, C.A., Vincent, A., Mathern, G.W., Cross, J.H., 2014. Rasmussen's encephalitis: clinical features, pathobiology, and treatment advances. Lancet Neurol. 13, 195–205.

Vezzani, A., 2015. Anti-inflammatory drugs in epilepsy: does it impact epileptogenesis? Expert Opin. Drug Saf. 14, 583–592.

Vezzani, A., Baram, T.Z., 2007. New Roles for Interleukin-1 Beta in the Mechanisms of Epilepsy. Epilepsy Curr. 7, 45–50.

Vezzani, A., French, J., Bartfai, T., Baram, T.Z., 2011. The role of inflammation in epilepsy. Nat. Rev. Neurol. 7, 31–40.

Vezzani, A., Friedman, A., Dingledine, R.J., 2012. The role of inflammation in epileptogenesis. Neuropharmacology 69, 16–24.

Vezzani, a, Conti, M., De Luigi, a, Ravizza, T., Moneta, D., Marchesi, F., De Simoni, M.G., 1999. Interleukin-1beta immunoreactivity and microglia are enhanced in the rat hippocampus by focal kainate application: functional evidence for enhancement of electrographic seizures. J. Neurosci. 19, 5054–5065.

Waisman, A., Liblau, R.S., Becher, B., 2015. Innate and adaptive immune responses in the CNS. Lancet Neurol. 14, 945–955.

Walsh, J.G., Muruve, D.A., Power, C., 2014. Inflammasomes in the CNS. Nat. Publ. Gr. 15, 1–14.

Webster, K.M., Sun, M., Crack, P., O'Brien, T.J., Shultz, S.R., Semple, B.D., 2017. Inflammation in epileptogenesis after traumatic brain injury. J. Neuroinflammation 14, 10.

Wirenfeldt, M., Clare, R., Tung, S., Bottini, A., Mathern, G.W., Vinters, H. V, 2009. Increased activation of Iba1+ microglia in pediatric epilepsy patients with Rasmussen's encephalitis compared with cortical dysplasia and tuberous sclerosis complex. Neurobiol. Dis. 34, 432–440.

Zhou, K., Shi, L., Wang, Y., Chen, S., Zhang, J., 2016. Recent Advances of the NLRP3 Inflammasome in Central Nervous System Disorders. J. Immunol. Res. 2016.